Department of Precision and Microsystems Engineering

A validation of a parametric compliance matrix for circularly curved leaf flexures and its application in parallel mechanisms

H.G. Miltenburg

Report no : 2023.083
Coach : Ir. A. Yaşir
Professor : Prof. Dr. Ir. J.L. Herder
Specialisation : Mechatronic System Design
Type of report : Master Thesis
Date : 4 October 2023

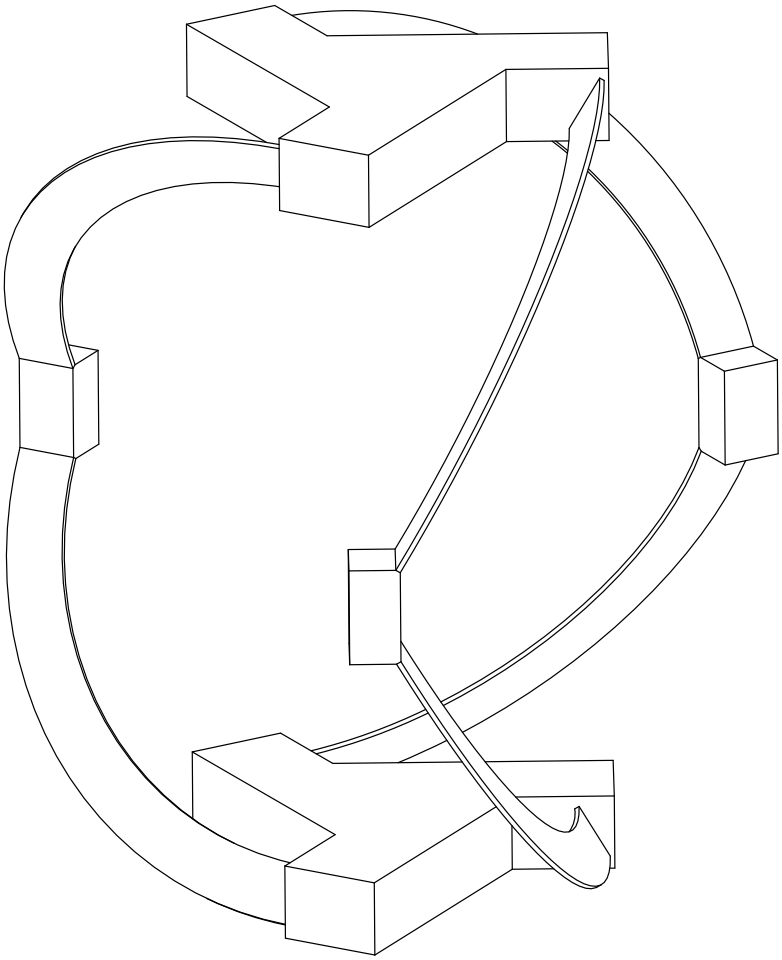

TU Delft Delft University of Technology

Challenge the future

A validation of a parametric compliance matrix for circularly curved leaf flexures and its application in parallel mechanisms

by

H.G. Miltenburg

to obtain the degree of Master of Science
at the Delft University of Technology,
to be defended publicly on Tuesday October 4, 2023 at 16:00.

Student number:	4394976	
Project duration:	September 5, 2022 – October 4, 2023	
Thesis committee:	Prof. Dr. ir. J.L. Herder,	TU Delft, supervisor
	Ir. A. Yaşir,	TBRM Engineering BV, daily supervisor
	Dr. D. Farhadi	TU Delft
	Dr. J. Jovanova	TU Delft

An electronic version of this thesis is available at http://repository.tudelft.nl/.

TU Delft

Preface

This master's thesis was written as part of the master Mechanical Engineering at the faculty of 3mE of the Technical University of Delft. Over the past year I worked on a research project concerning flexures with an initial curvature, which resulted in two papers that are presented in this report. In the first part of the project a literature study was conducted. The goal was to create an overview of the relevant literature on initially curved flexures and their applications in compliant mechanisms. In the second part of the project, research was conducted to cover one of the research gaps identified in the literature study. The findings of the first and second part can be found in paper I and paper II respectively.

Contents

Preface **1**

1 Paper I: An overview of initially curved flexures in compliant mechanisms **3**

2 Paper II: A validation of a parametric compliance matrix for circularly curved leaf flexures and its application in parallel mechanisms **17**

Chapter 1

Paper I: An overview of initially curved flexures in compliant mechanisms

An overview of initially curved flexures in compliant mechanisms

H.G. Miltenburg

24/02/2023

Abstract

Initially straight beam flexures (SBF) are commonly used in compliant mechanisms. This paper presents an overview of initially curved beam flexures (ICBF) to asses their application in compliant mechanisms. Relevant literature is reviewed that discusses initially curved beams or the use of ICBFs in compliant mechanisms. The results are categorized by the shape of the curvature and by the function of the compliant mechanism. It shows that parasitic motions and maximum stresses can be reduced and that the range of motion can be improved when ICBFs are used instead of SBFs. Also, the geometry of the curvature results in an increase of design space, making it possible to create mechanisms that would not be possible with SBFs. An overview of the existing methods of modeling ICBFs, as well as design methodology is also presented in this paper.

1 Introduction

Mechanisms are used to transform force, motion, and energy. In rigid body mechanisms, this happens through rigid links and joints based on rolling or sliding contacts. Compliant mechanisms achieve their motion through elastic deformation of their flexure joints [1]. This has several advantages [2]. The mechanisms can be monolithic, reducing the number of parts, which lowers manufacturing costs and assembly time. The movement of the mechanism happens through elastic deformation instead of rigid body joints, which eliminates friction forces associated with rubbing surfaces. Friction-free motion also makes lubrication obsolete, as there is no more wear. Therefore, compliant mechanisms could be a solution for applications in environments that do not allow wear or lubrication, such as vacuum or biomedical implants. The absence of friction and backlash in compliant mechanisms makes them ideal for high-precision applications. With the motions being wear-free, it is possible to create motions with high reliability and repeatability.

However, compliant mechanisms also present challenges. As motion happens through elastic deformation, the range of motion is limited and fatigue should be considered. Just like in rigid-body mechanisms, parasitic motions occur. Parasitic motions are secondary displacements that are dependent on other independent primary displacements. The primary compliance of a mechanism describes the relation between the primary load and the primary displacement. The relation between this primary load and the secondary displacements is called the secondary compliance [3], or inter-directional coupling [4]. When such coupling between different directions of deformations is not present in a mechanism, it is called a decoupled mechanism.

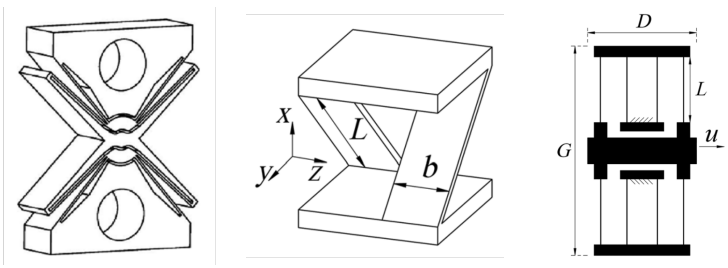

(a) (b) (c)

Figure 1: Compliant joints containing SBFs: (a) Butterfly compliant revolute joint, (b) cross-axis compliant revolute joint, and (c) symmetrical double block compliant translational joint [1]

A leaf spring is a widely applied flexure joint in compliant mechanisms. Many compliant joints reviewed in [1] use one or more leaf springs to achieve the desired mobility, such as the butterfly revolute joint, the cross-axis compliant revolute joint, or the symmetrical double block compliant translational joint (Figure 1). The leaf springs in these compliant joints are initially straight, also known as straight beam flexures (SBF). To a lesser extent, designs have been made using initially curved beam flexures (ICBF). The initial curvature of the flexures increases the design space for the designer, making it possible to design mechanisms with features that can't be achieved with SBFs [5]. Literature on ICBFs exists, however, it is scattered, and the difference between shapes of curvatures are not properly defined.

The aim of this literature review is to create an overview of the effect an initial curvature has on the mechanical behavior of beam flexures, and how these curvatures are used in the design of compliant mechanisms. Furthermore, different methods for modeling initially curved beams will be reviewed.

This literature review will focus on beam flexures with a curved geometry that exists in a plane before deflection. First, the approach strategy of this literature study is explained in section 2. Afterwards, in section 3, the reviewed literature is presented, followed by a discussion and a conclusion.

2 Method

2.1 Search method

In order to create an overview, a literature study was done. The relevant literature was searched using Google Scholar and Scopus. In order to find the most relevant articles, a set of search terms were used with Boolean operators "AND", and "OR". Keywords "Flexure" or "Beam" were used in combination with "Curved" or "Initially curved". Some authors indicate the shape of curvature rather than using the term "Curved". In order to include these results alternative search terms were used, such as "Cylindrical", "Circular", "Elliptical", "Parabola" etc.

Beams are not exclusively used in compliant mechanisms. Therefore, in order to find literature where initially curved beams are applied in compliant mechanisms, the search term "compliant mechanism" can be added. However, as literature outside of the field of compliant mechanisms can be relevant to this overview, both searches with and without the search term "compliant mechanism" have been made.

Searching *"curved" AND "beam"* resulted in > 1000000 results in Google Scholar. Adding *"initially" AND "compliant mechanism"* narrows the results down to several hundred results. Relevant papers could lead to other relevant papers through their own references. Many results merely mention ICBFs and focus on different aspects. For this overview, the focus is on literature that more substantively discusses the effects and applications of ICBFs.

2.2 Classification

With the method described above different papers were found ranging from designs using ICBFs to presenting methods for modelling beams with an initial curvature. In order to create an overview, the papers need to be classified. Initially, a classification is made based on the shape of the curvature. This results in an overview that shows the different shapes of curvature that are being used in compliant mechanisms in the literature, and the characteristics associated with these particular shapes. Next to the different shapes and their applications, an overview is desired that presents the different methods that are being used in modelling beams with an initial curvature. Therefore the models presented in the literature will be classified by its respective method of modelling.

3 Results

As proposed in section 2, the initially curved beam flexures will be classified based on the shape of curvature. Furthermore, beam flexures can be divided into two types of deformation: in-plane and out-of-plane deformation. Both types of deformation cover, as their names suggest, the deformations where the beam flexure remains within the initial plane of curvature and the deformations that move the beam flexure out of the initial plane of curvature respectively. Two examples of beam flexures experiencing in-plane and out-of-plane deformations are portrayed in Figure 2. Both beam flexures have the same curvature, however, due to a different I_r/I_z ratio, Figure 2a has a high in-plane compliance and Figure 2b has a high out-of-plane compliance. By applying an

out-of-plane load, a torque is introduced that is not present in the in-plane deformations. This torque results in a twist along the beam's length.

For all flexures with an initial curvature applies that the curvature increases the effective length of the beam while maintaining the distance between its base and its end-effector. According to Euler-Bernoulli beam theory, the angle of deflection can be determined by $\theta = \frac{ML}{EI}$, and by increasing length L, the angle of deflection also increases, creating a larger range of motion (ROM) [6].

3.1 Types of curvature

3.1.1 Circularly curved beam flexures

Circularly Curved-Beam Flexures (CCBF) have a constant radius R over a certain sweep angle Φ. As depicted in Figure 2, depending on its I_r/I_z ratio the beam flexure is compliant for in-plane or out-of-plane deformations. Consequently, the in-plane CCBFs are mainly exclusively used for planar mechanisms, while the out-of-plane CCBFs are mostly used for spatial mechanisms.

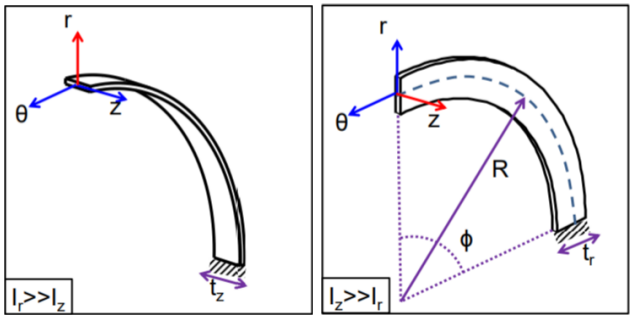

(a) (b)

Figure 2: CCBF for (a) in-plane deformations and for (b) out-of-plane deformations [7]

In-plane deformation CCBFs

The in-plane deformation CCBFs can be parameterized such that it either has a high compliance in $r-$ or $\theta-$direction. As shown by Telleria [7], an equal compliance in both directions can be achieved. Parasitic motions for these primary displacements are the translation in the other planar direction and the angular displacement around the z-axis.

The CCBF is compared to an SBF for the application in planar revolute joints by Berselli et al.(Figure 3a) [8]. After setting up the compliance matrix for both an SBF and a CCBF, indexes are proposed to quantitatively evaluate both the selective compliance and the maximum achievable rotation. The range of parameters that are evaluated in this paper shows an increase in ROM for the CCBF, but also an increase in parasitic motions. Verotti [11] evaluated the effects an initial curvature has on the positioning accuracy for revolute joints. This

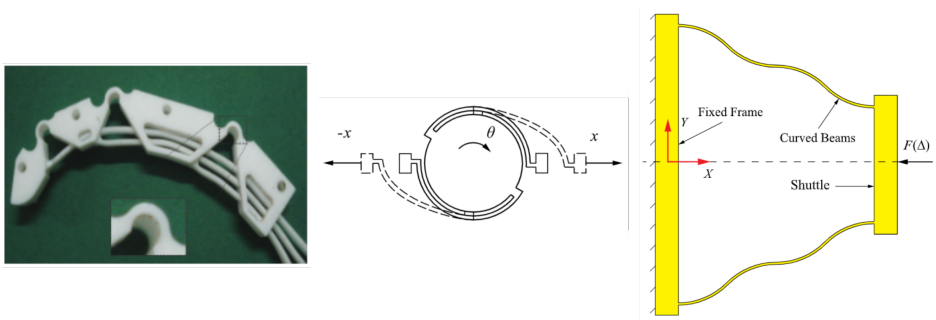

(a) (b) (c)

Figure 3: R-compliance CCBFs in compliant mechanisms: (a) Planar revolute joint [8], (b) Pure rotation micro-positioning stage [9], (c) Corrugated CCBFs for a quasi-constant force output [10]

is done for a range of values for radius R and sweep angle Φ over a large range of deformation. It shows that axis drift can be limited by increasing the sweep angle, however, the sweep angle should be chosen carefully as the x and y components of the axis drift are impacted differently by the sweep angle of the initial curvature. Therefore, it can not be said that an increasing sweep angle generically results in a decreasing axis drift. It is shown that the positioning errors can also be reduced using an initial curvature. Not only the geometrical parameters but also the direction and the magnitude of the deflection influence the determine the reduction in positioning errors. In this study, stresses are not considered and therefore no conclusions can be made about the range of motion.

Zhang et al. [9] designed a circular pure rotation micro-positioning stage using CCBFs. It is stated that the resolution of such mechanisms is usually compromised for an increasing ROM. To counter this problem, a dual-stage compliant mechanism is proposed, where both stages are compliant slider crank mechanisms. For the coarse stage lumped compliance design methodology is used, using notched hinges. The fine positioning stage uses distributed compliance design methodology, using two CCBFs. By placing two CCBFs symmetrically as shown in Figure 3b, a pure rotation is created from a translational input. Compared to using notched hinges, this gives a lower output-to-input rate, making it more suitable for low ROM but high-resolution applications. Additionally, it is more compact. Therefore a lumped compliance mechanism is used for the large ROM, low-resolution stage, and the distributed compliance mechanism (using CCBFs) is used for the fine rotation stage.

A mechanism was created by Zhang et al. [10] that uses corrugated chains of CCBFs that have a quasi-constant force output with a large displacement. Figure 3c.

Out-of-plane deformation CCBF

The out-of-plane deformation CCBFs experience a torque that is absent in SBFs when being actuated in the z-direction. This torque results in a twist along the length of the beam. For a primary displacement in the z-direction, the CCBF therefore has an additional parasitic motion around the $\theta-$axis, when compared to SBFs [5].

Parvari Rad et al. [3] investigated the use of CCBFs for a Spherical Compliant Mechanism (SCM). The SCM that is proposed consists of a serial chain of three identical CCBFs orientated such that they share the same

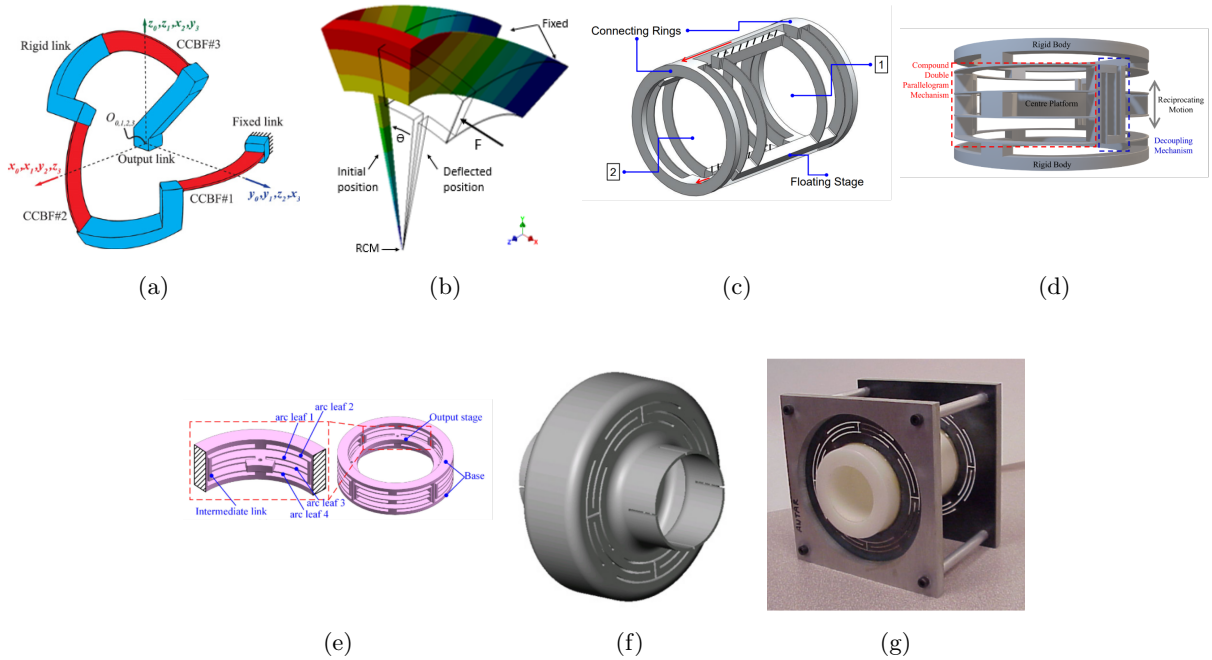

Figure 4: Z-compliance CCBFs in compliant mechanisms: (a) Spherical compliant mechanisms [3], (b) Rotational parallel mechanism with a remote center of rotation [12],(c, d, e) Cylindrical compliant linear guide [13] [14] [7], (f) 5-DoF flexible coupling [15], (g) 1-DoF linear guide [15]

center of curvature, as shown in Figure 4a. When compared to an equivalent SCM that uses SBFs and has an identical primary rotational compliance, an SCM with CCBFs shows a decrease in parasitic motions. With this knowledge, a parametric study has been conducted on the SCM using CCBFs. It is concluded that for a fixed primary compliance factor, the secondary compliance factors can be minimized by increasing the t_r/t_z ratio and sweep angle ϕ, and decreasing radius R.

Van Houten [12] used two z-compliance CCBFs to create a parallel mechanism with a rotational DOF with a remote center of motion (Figure 4b). Using finite element analysis (FEA) the mechanism is compared to the equivalent mechanism using SBFs. It is shown that using CCBFs rather than SBFs reduces the axis drift and the maximum stress in the flexure. Through parametric analysis using FEM it is shown that by decreasing sweep angle ϕ and radius R, and by increasing width w and the angle between the two beam flexures α, the parasitic errors of the mechanism can be reduced. This however also increases the rotational stiffness.

Several cylindrical compliant prismatic joints have been proposed using CCBFs [7] [14] [13], shown in Figure 4c, 4d and 4e respectively. Telleria [7] developed design guidelines for CCBFs, on an elementary level and on how to combine these elements in a parallel/serial configuration for cylindrical mechanisms. In subsection 3.3 they are discussed in more detail. These guidelines were used to create a cylindrical compliant linear guide comprising of two parallelogram flexure mechanisms using CCBFs (Figure 4c). The design was compared with an existing mechanism. Using CCBFs allows a cylindrical mechanism. The manufacturing costs were significantly lowered, as it is possible to manufacture the mechanism from precision round stock. The ROM-to-footprint ratio is higher and the tip and tilt parasitic motions respect the same functional requirements as the existing design. Additionally, the cylindrical shape of the mechanism makes it axial symmetric, decreasing the effect of load placement errors, and the overall parasitic displacement. Symmetry can also offer thermal insensitivity. The cylindrical shape of the mechanism can also be beneficial for certain applications, such as opto-mechatronics. The circular objectives can be manipulated by the cylindrical mechanism, while light can travel through its center.

Awtar and Slocum [15] showed the potential of CCBFs by designing both a 5-DOF flexible coupling and a 1-DOF linear guide, as depicted in Figure 4f and 4g. It is stated that nonlinear elastokinematic effects are more dominant in CCBFs with out-of-plane deformations when compared to SBFs, causing the off-axis stiffness of the CCBFs to decrease faster with increasing out-of-plane deflection.

3.1.2 Elliptical shaped curved beam flexures

Dearden et al. [16] introduced a cylindrical-shaped flexure joint based on the cross-axis flexure joint (Figure 5a). This design uses elliptical-shaped flexures with a variable cross-section. The cylindrical geometry allows for cables to pass through the center of the flexure joint, which is necessary to actuate minimal invasive surgery instruments that are often located at the end of cylindrical shafts. This flexure joint using elliptical flexures shows to increase the off-axis stiffness when compared to a comparably sized flexure joint using straight flexures.

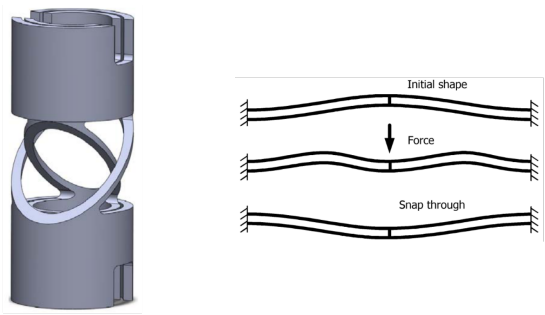

(a) (b)

Figure 5: (a) Elliptical shaped beam flexure in a cylindrical shaped flexure joint [16], (b) Cosine shaped curved beam flexure in a bistable mechanism [17]

3.1.3 Cosine-shaped curved beam flexures

By giving two parallel beams an initial cosine-shaped curve, and by connecting them in the center (Figure 5b), a bistable mechanism can be made that does not need any hinges, latches or residual stresses in the material [17].

3.1.4 Spline-shaped curved beam flexures

Splines and Bézier curves are parametric mathematical expressions describing the shape of a complex curvature. It has been incorporated in the design of curved beam flexure elements in compliant mechanisms [4] [18] [4]. By using beam elements with an initial spline curvature, Lin et al [4] were able to create a relatively simple 6-DoF compliant mechanism (Figure 6a). It is stated that the use of initially curved beams solves the contradiction of a simple structure with multiple degrees of freedom, however, the mechanism has inter-directional coupling rates up to a maximum of 12%.

Prakashah and Zhou [18] created a mechanism with a constant output torque for a large range of input rotation. The mechanism consists of a fixed ring with an input shaft in its center, as shown in Figure 6b. Spline shape curved beams are used to connect both parts, the number of beams can be decided by the designer based on practical reasons. The mechanism has an average output torque error of 2.6 Nmm for a desired input torque of 100 Nmm for a rotation between 20-60 °.

Jutte and Kota [19] developed a generalized synthesis method to create mechanisms with a specific load-displacement curve, using splines to determine the initial curvature of the flexure beams. The method proved successful in creating mechanisms with constant force behavior or linear spring behavior over large ranges of motion. Figure 6c shows a mechanism with linear stiffness behavior.

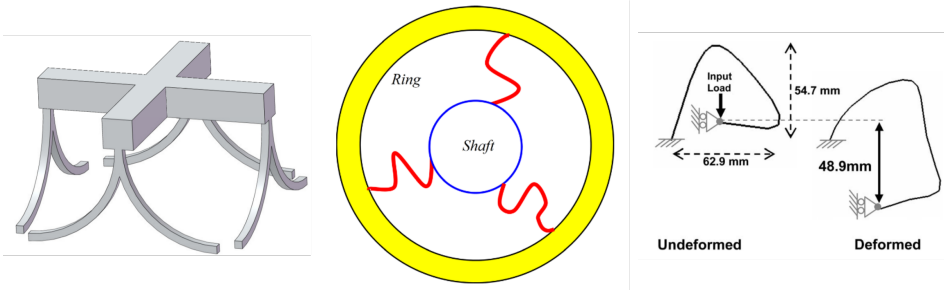

(a) (b) (c)

Figure 6: Spline shaped curvatures in compliant mechanisms: (a) 6 DoF compliant mechanism [4], (b) Constant output torque mechanism [18], (c) Linear stiffness over a large RoM [19]

3.2 Modeling methods

A model is a mathematical representation of the mechanical behavior of a physical mechanism and is used to analyze or synthesize designs. This section presents different methods that are used in the literature to model beams with an initial curvature. The Finite Element Method (FEM) is a popular method for modeling compliant mechanisms, as it accurately covers many different shapes, and also evaluates stresses. However, parametric analytical models are preferred, as they do not need a lot of computational resources [20] and present a transparent relation between the parameters and the behavior of a mechanism.

3.2.1 PRBM

The motion of a compliant mechanism can be estimated by beam deflection equations, which can be highly complex and nonlinear. These equations can be reduced to simpler nonlinear algebraic equations using a pseudo-rigid-body model (PRBM), making analysis and design simpler. A PRBM is a numerical approximation of a compliant element that offers a rigid body mechanism that resembles the compliant mechanism. This rigid body mechanism consists of rigid links and revolute joints with torsional springs. The stiffness of the compliant mechanism is captured by these springs and the deflection path is represented by the kinematics of the rigid links. PRBMs are able to capture large deformations with short computation times when compared to FEM. PRBMs have been developed for different kinds of compliant elements, including many flexure joints. To a lesser extent, PRBMs have been presented that cover beams with an initial curvature.

Venkiteswaren et al. [21] introduce a PRBM for circular beams under combined tip loads for in-plane deformations. First, the beam equations for a circular beam are derived. By calculating the deflection of the beam tip with these equations, it can be seen that the deflected location of the beam tip lies in an arc shape.

The approximate center of this arc is the location of the first revolute joint of the PRBM that is connected to the base by the first rigid link. The location of the second revolute joint is at the end of the second rigid link, and thus at the beam tip. This second revolute joint makes it possible to not only determine the deflection of the beam tip, but also its orientation. The PRBM is defined by four parameters, the initial angles of the rigid links and the rotational stiffnesses of the two revolute joints. Equations for these parameters have been determined by an optimization script that minimizes the error between the PRBM and the beam equations. The error of the PRBM when compared with FEA is between 1 and 5%. As the PRBM is based on the beam equations, it is only applicable to slender beams with a constant cross-section along its main axis.

This model was later expanded by modeling the initially curved beam as four rigid links with three revolute joints (3R) to cover a broader range of curvatures. By making use of symmetry this PRBM can be expressed by only three independent parameters. This model is not only able to represent circular beams, but also straight beams. It is also shown that single-loop fully compliant mechanisms can be analyzed using this model in combination with loop equations. Additionally, a methodology is presented for the analysis and synthesis of compliant mechanisms containing both circularly curved and straight beams, using the 3R PRBM. The PRBM is not able to calculate stresses in the beams and is limited to slender beams with in-plane deformations.

3.2.2 Beam constraint model (BCM)

The beam constraint model (BCM) [22] is a mathematical model based on Euler-Bernoulli beam theory that can be used to accurately capture closed-form equations describing the nonlinear load-displacement relations for beams with small initial circular curvature (length $L < 10\%$ of radius R). For displacements within 10% of its length and a maximum allowable tangential force on the tip of the beam nonlinear kinematic, nonlinear load-stiffening, and nonlinear elastokinematic effects are captured accurately, which enables the accurate prediction of error motions and stiffness properties. As the model is based on the Euler-Bernoulli beam theory, it is only applicable to slender beams.

Chen et al. [23] propose the chained beam constraint model (CBCM), which discretizes an initially curved beam into different circular elements. These elements can be of different radii, but should all be of approximately equal length. Each of these elements is modeled using BCM. As any curvature can be discretized into a certain amount of circularly curved beams, CBCM is able to model initially curved beams of various shapes. However, as the length of the elements should remain approximately equal, the shapes are somewhat limited. Discretization also eliminates the restriction of small deflection, small initial curvature, and a maximum allowable tangential tip force, which should be regarded in BCM. CBCM is validated using nonlinear FEA, which showed a maximum error of $< 0.15\%$. The computation time for the same calculation is 14.76 s and 12.79 s for FEM and CBCM respectively.

3.2.3 Compliance matrix

A compliance matrix is a matrix that shows the relation between the loads and the displacements of the free end of the beam for small deformations, $D = C_s F$ [24] with

$$D = [x \quad y \quad z \quad \theta_x \quad \theta_y \quad \theta_z]^T, \quad F = [F_X \quad F_Y \quad F_Z \quad M_X \quad M_Y \quad M_Z]^T$$

$$C_S = \begin{bmatrix} C_{S11} & C_{S12} & C_{S13} & C_{S14} & C_{S15} & C_{S16} \\ C_{S21} & C_{S22} & C_{S23} & C_{S24} & C_{S25} & C_{S26} \\ C_{S31} & C_{S32} & C_{S33} & C_{S34} & C_{S35} & C_{S36} \\ C_{S41} & C_{S42} & C_{S43} & C_{S44} & C_{S45} & C_{S46} \\ C_{S51} & C_{S52} & C_{S53} & C_{S54} & C_{S55} & C_{S56} \\ C_{S61} & C_{S62} & C_{S63} & C_{S64} & C_{S65} & C_{S66} \end{bmatrix}$$

The elements of the matrix can be obtained in several ways, such as The Maxwell-Mohr method [24], Castigliano's second theorem [7] [13], and the direct method [8] [3]. The references show the derivations in more detail. Wu et al. [24] use the Maxwell-Mohr method to derive the elements of C_S. The compliance matrix is then verified by FEA for three cases, a beam with an archimedean-spiral curvature, a circularly curved beam, and a circularly curved beam with a varying cross-section. Linear FEA is chosen, as the compliance matrix is only valid for small deformations and does not capture material nonlinearity and geometric nonlinearity. The maximum error is below 3 % and the computation time of the analytical model is less than $1/60^{th}$ of the computation time needed for FEA.

The compliance of the serial linkage of flexure elements shown in Figure 4a can be obtained by the sum of the compliance matrix of each flexure element, provided that these matrices are expressed in a common reference frame [3], which can be achieved using transformation matrices.

3.3 Design methods

For compliant mechanisms using SBFs, several useful tools exist that help in the design process. A conceptual design can be made based on an existing mechanism, or through the use of a building block approach or freedom and constraint topology [20]. However, these methods do not cover beam flexures with an initial curvature. This results in many designs being based on existing SBF designs, or in designs where the conceptual design phase is left out as a whole. After the concept selection, it is common to use an optimization method to achieve the desired mechanism. The optimization algorithm evaluates the initial design and changes the variable parameters until the mechanism shows the desired characteristics. The evaluation can be done using any of the models described in subsection 3.2. The variable parameters in the constant torque mechanism (Figure 6b) for example, are the interpolation circles that describe the spline curve of the beam flexures. Each interpolation circle contains two coordinates and a diameter that describes the location of the interpolation circle and the width of the beam at that point respectively. The rest of the spline is determined by interpolation. The initial design is a random set of interpolation circles. The objective function is the average of the actual output torque minus the desired output torque. FEA is used to evaluate the performance of each iteration. Minimizing this objective function by optimizing the variable parameters results in a constant torque mechanism. Another way of synthesis happens through conducting a parametric study and choosing the dimensional parameters best suited for the application of the mechanism [8].

In her PHD thesis, Telleria proposes a set of design guidelines for cylindrical mechanisms with CCBFs [7]. By revealing the key parameters of the compliant matrix for a single CCBF, a better understanding of the mechanical behaviour is generated. Not only the effect that the parameters have on the stiffness ratios and the parasitic motion ratios are studied, but also the effect of load location, and boundary conditions. This gives designers fundamental knowledge on how to design CCBFs. Next to these guidelines on an elemental level, guidelines on assembling these elements into a cylindrical system are proposed. These guidelines contain an approach on how to determine the compliance matrix of a cylindrical system and how to form equations to model the parasitic motions of the end effector. The effects different system parameters, such as the distance between the beam flexure elements or the load location, have on the parasitic ratios of the end effector are evaluated. This knowledge on the key parameters of CCBFs and how it impacts the performance of the mechanism is essential to rapidly generate and optimize designs. To validate the guidelines, a cylindrical compliant linear guide with one DOF is designed, which is described in subsection 3.1.

3.4 Combined results

The literature that is presented in above shows a variety in both the shape of curvature and its application in compliant mechanisms. In order to create a visual overview of the literature, the results have been presented in Table 1 according to their classification. The shapes of the curvature are assigned in the rows of the table. The columns indicate the function or application of the compliant mechanism discussed in the respective paper. This can either be a case of a kinematic pair, a desired load-deflection curve or another application. The table also includes the remarks that were made by the authors of the paper, either on the benefits (in green) or the limitations (in red) of using initially curved beam flexures for the specific application.

The different methods for modeling that are described in the literature are combined in Table 2, to provide an overview and to summarize the most important features of each method.

Table 1: An overview of ICBFs with different shapes of curvatures, their applications, and their features compared to equivalent mechanisms using SBFs

Shape of curvature \ *Function*	**Revolute joint**	**Prismatic joint**	**Spherical joint**	**Load-deflection**	**Other**
CCBF in-plane deformation	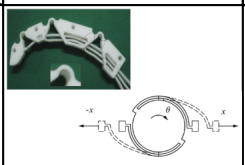 [8] [9] [10] +Increased ROM +Decreased parasitic motion +Decreased positioning errors			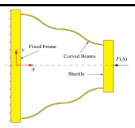 [11]	
CCBF out-of-plane deformation	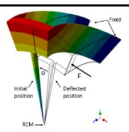 [12] +Decreased maximum stresses +Decreased parasitic motion	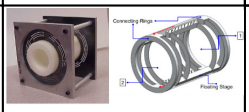 [7] [13] [14] [15] +Reduced manufacturing costs and time +Increased ROM/footprint ratio +Cylindrical geometry	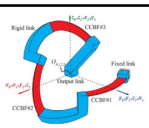 [3] +Reduced parasitic motions		 [15] - Faster decrease of off-axis stiffness after deflection
Elliptical	[16] +Cylindrical geometry +Increased off-axis stiffness				
Cosine					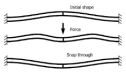 [17] +Bistable mechanism without hinges, latches or residual stresses
Spline				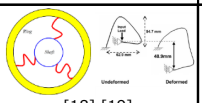 [18] [19] +Constant force/torque behaviour over a large ROM	 [4] +Relatively simple mechanism with 6 DOF - High inter-directional coupling

Table 2: An overview of different methods used to model initially curved beam flexures and FEM

Method	**References**	**Deformation**	**Shape of curvature**	**Error**	**Advantages**	**Disadvantages**
PRBM	[21] [25]	In-plane	Circular	$\approx 1\%$[1]	Short computation time Large ROM	Limited to slender beams
CBCM	[22] [23]	In-plane	Circular and non-circular shapes (limited by discretization)	$< 0.15\%$	Captures nonlinearities Large ROM	Limited to slender beams Computation time similar to FEM
Compliance matrix	[3] [7] [8] [13] [24]	In-plane Out-of-plane	Any 3D general curve [26]	$< 3\%$	Short computation time Clear presentation of secondary compliances	Small ROM Does not capture nonlinearities
FEM		In-plane Out-of-plane	Any 3D shape	-	Captures nonlinearities Large ROM Shows stress and stress concentrations	Long computation time No insight on parametric sensitivity

[1] Derived from the results in [25]

4 Discussion

From Table 1 it can be concluded that substantially more research has been done in CCBFs than in any other shape of curvature. This could be explained by the fact that this is the most simple shape of curvature, with only two additional parameters. Besides, the knowledge gained on CCBFs can up to a certain extent be generalized over other shapes of curvature. Eventually, when a good understanding of the behavior of CCBFs is achieved, the literature density evens out over the other shapes of curvature.

There seem to be a few reasons for using initially curved beam flexures in compliant mechanisms. An obvious feature is the geometrical shape of the curvature. With an initial curvature, the design space is increased. This allows designers to work around geometrical constraints in the mechanisms. The increased design space can be noticed in the high interest in cylindrical-shaped mechanisms. This geometry is beneficial for certain applications, like opto-mechatronics or minimal invasive surgery, but also allows an axial symmetry, which can reduce load placement errors and offers thermal insensitivity. Additionally, manufacturing costs and time can be reduced due to the availability of round stock. Within this cylindrical shape, the ICBFs take up less space than SBFs with the same ROM, resulting in an increase of the ROM over footprint ratio. Additionally, the performance of the flexures can be improved by using an initial curvature. It has been shown that initially curved beam flexures show potential in reducing parasitic motions in spherical and revolute joints. It should be noted that this is not a generic conclusion and depends on the values that are used for the key parameters, but also on the load case. Assembling initially curved beam flexures in parallel mechanisms allows further reduction of parasitic motions in revolute joints. Another feature that exists in all beams with an initial curvature is the longer effective length between the base and end effector on either side of the beam when compared to SBFs. This increase in effective length distributes the stresses more evenly over the beam, resulting in lower peak stresses and increased ROM. The literature also presents several cases where the nonlinear nature of the mechanics of initially curved beams has been used to create specific load-deflection curves, such as constant torque or linear stiffness. Splines seem to be a suitable choice as it allows complex shapes with simple parameters. Optimization is used to iterate the shape of the spline until it performs as desired.

An initially straight beam has a high stiffness along the length of the beam, and therefore acts as a line constraint between the two points at the end of the beam when buckling is not considered. For an initially curved beam that is designed for in-plane deformations, the stiffness in the line between the two points is decreased by the curvature. The initially curved beam therefore acts more like a prismatic joint with a certain stiffness than a line constraint in this direction.

As described above, ICBFs can outperform SBFs in parasitic motions, range of motion, and peak stresses. The key parameters that influence these features have been identified. The off-axis stiffness is less mentioned in the literature. It is said that the off-axis stiffness of CCBFs decreases faster for out-of-plane deformation than similar SBFs, but this is not quantified. Additionally, the off-axis stiffness of the cylindrical cross-axis revolute joint of Figure 5a is said to be higher than its SBF equivalent. However, it is not explained what parameters cause this difference.

The available methods for modeling are presented in Table 2, with their respective characteristics. Next to FEM, three different methods for modeling beams with an initial curvature were found in the literature. These methods can be evaluated by the error with respect to FEM, the shapes of the beam and the curvature covered by the method, and the computation time. Not all methods are suitable for the same analysis, they all have their advantages and disadvantages. For out-of-plane beam deformation, the compliance matrix seems to be the only suitable choice. However, this method is limited to small ROM. For large in-plane deformation analysis, both PRBM and CBCM are suitable. Using CBCM, the lowest error can be achieved. However, CBCM is restricted by covering just a certain range of loads and shapes of curvature. For the analysis of a mechanism, it can be chosen to use multiple methods for modeling. The different models complement each other, making it possible to work around the disadvantages of each method. For out-of-plane deformations, this is not possible, as only the compliance matrix is available. Since the compliance matrix is unable to cover large deformations, FEM would be needed to evaluate large ROM. FEM should also be used to evaluate the stresses in the compliant mechanisms, as this can not be done by the other methods.

Design methods that are used in compliant mechanisms using SBFs do not always work for ICBFs. Methods for conceptual design are clearly missing from the literature, which hinders the use of initially curved beam flexures in compliant mechanisms. Most designs in the literature are either arbitrary or based on existing designs, before being optimized using existing techniques. Design rules are introduced by Telleria [7] to gain an understanding of the key parameters of CCBFs and how to use them in serial or parallel cylindrical mechanisms,

making it possible to create the cylindrical prismatic joint as depicted in Figure 4c. Van Houten analyzed the axis drift of a rotational mechanism containing two CCBFs in parallel [12] using FEM. Whereas the behavior of individual CCBFs is fairly well understood, knowledge of assembling multiple CCBFs in parallel mechanisms is lacking in the literature.

5 Conclusion

In this literature survey, an overview is created of ICBFs with different shapes, their behavior, and their application in compliant mechanisms. It is concluded that several reasons exist for using ICBFs over SBFs. It has been shown that the use of ICBFs can result in an increase in range of motion, a decrease in parasitic motion, and decreased peak stresses. Also, the shape of the flexure results in an increased design space. This makes it for example possible to create mechanisms with circular or cylindrical geometry. Papers are presented that identify the relation between the different parameters and the desired behavior, allowing parametric optimization. The overview also indicates where the literature is less densely researched, such as methods for the conceptual design phase, and the behavior of parallel mechanisms using ICBFs.

This literature also presents an overview of the methods that are being used for modeling the ICBFs. Different methods are presented, each having its advantages and limitations. Where PRBM, and CBCM are capable of modeling large deflections, they can be used exclusively in planar mechanisms. The compliance matrix is able to model out-of-plane deformations, and can therefore be used in spatial mechanisms, however, this method is limited to small deflections.

References

[1] D. Farhadi, N. Tolou, and J. Herder, "A review on compliant joints and rigid-body constant velocity universal joints toward the design of compliant homokinetic couplings," *Journal of Mechanical Design*, vol. 137, p. 032301, 03 2015.

[2] L. L. Howell, *Handbook of Compliant Mechanisms.* John Wiley & Sons Ltd., 2013, ch. 1, pp. 3–13.

[3] F. Parvari Rad, G. Berselli, R. Vertechy, and V. Parenti-Castelli, "Design and stiffness analysis of a compliant spherical chain with three degrees of freedom," *Precision Engineering*, vol. 47, pp. 1–9, 2017. [Online]. Available: https://www.sciencedirect.com/science/article/pii/S0141635916300897

[4] S. Lin, J. Wang, W. Xiong, Q. Hu, H. Liu, and Q. Wang, "Design and modeling of a curved beam compliant mechanism with six degrees of freedom," *Micromachines*, vol. 13, no. 2, 2022. [Online]. Available: https://www.mdpi.com/2072-666X/13/2/208

[5] M. J. Telleria and M. L. Culpepper, "Understanding the drivers for the development of design rules for the synthesis of cylindrical flexures," *Mechanical Sciences*, vol. 3, pp. 25–32, 2012.

[6] N. Wang, X. Liang, and X. Zhang, "Pseudo-rigid-body model for corrugated cantilever beam used in compliant mechanisms," *Chinese Journal of Mechanical Engineering (English Edition)*, vol. 27, pp. 122–129, 1 2014.

[7] M. J. Telleria, "Design rules and models for the synthesis and optimization of cylindrical flexures," Ph.D. dissertation, Massachusetts Institute of Technology, 2013.

[8] G. Berselli, F. Parvari Rad, R. Vertechy, and V. Parenti Castelli, "Comparative evaluation of straight and curved beam flexures for selectively compliant mechanisms," in *2013 IEEE/ASME International Conference on Advanced Intelligent Mechatronics*, 2013, pp. 1761–1766.

[9] J. Zhang, J. Gan, H. Ding, and H. Li, "Design of a pure rotation micropositioning stage with dual-range," *Mechanism and Machine Theory*, vol. 169, p. 104631, 3 2022.

[10] Q. Zhang, P. Yan, and H. Wang, "A curved-beam based quasi-constant force mechanism supporting large range and force-sensitive robotic manipulation," *Mechanism and Machine Theory*, vol. 172, p. 104799, 6 2022.

[11] M. Verotti, "Effect of initial curvature in uniform flexures on position accuracy," *Mechanism and Machine Theory*, vol. 119, pp. 106–118, 2018. [Online]. Available: https://www.sciencedirect.com/science/article/pii/S0094114X17309059

[12] A. Van Houten, "Rcm mechanism based on curved flexures," Master's thesis, TU DELFT, the Netherlands, 2021.

[13] M. Yang, C. Zhang, X. Huang, S. L. Chen, and G. Yang, "A long stroke nanopositioning stage with annular flexure guides," *IEEE/ASME Transactions on Mechatronics*, vol. 27, pp. 1570–1581, 6 2021.

[14] T. Liu and G. Hao, "Design of a cylindrical compliant linear guide with decoupling parallelogram mechanisms," *Micromachines*, vol. 13, no. 8, 2022. [Online]. Available: https://www.mdpi.com/2072-666X/13/8/1275

[15] S. Awtar and A. H. Slocum, "Flexure systems based on a symmetric diaphragm flexure," 2005.

[16] J. Dearden, C. Grames, J. Orr, B. D. Jensen, S. P. Magleby, and L. L. Howell, "Cylindrical cross-axis flexural pivots," *Precision Engineering*, vol. 51, pp. 604–613, 1 2018.

[17] J. Qiu, J. H. Lang, and A. H. Slocum, "A curved-beam bistable mechanism," *Journal of Microelectromechanical Systems*, vol. 13, no. 2, pp. 137–146, 4 2004.

[18] H. N. Prakashah and H. Zhou, "Synthesis of constant torque compliant mechanisms," *Journal of Mechanisms and Robotics*, vol. 8, 12 2016.

[19] C. V. Jutte and S. Kota, "Design of nonlinear springs for prescribed load-displacement functions," vol. 130, 8 2008, pp. 0 814 031–08 140 310.

[20] P. Bilancia and G. Berselli, "An overview of procedures and tools for designing nonstandard beam-based compliant mechanisms," *CAD Computer Aided Design*, vol. 134, 5 2021.

[21] V. K. Venkiteswaran and H. J. Su, "Pseudo-rigid-body models for circular beams under combined tip loads," *Mechanism and Machine Theory*, vol. 106, pp. 80–93, 12 2016.

[22] S. Awtar and S. Sen, "A generalized constraint model for two-dimensional beam flexures: Nonlinear load-displacement formulation," *Journal of Mechanical Design, Transactions of the ASME*, vol. 132, pp. 0 810 081–08 100 811, 8 2010.

[23] G. Chen, F. Ma, G. Hao, and W. Zhu, "Modeling large deflections of initially curved beams in compliant mechanisms using chained beam constraint model," *Journal of Mechanisms and Robotics*, vol. 11, 2 2019.

[24] K. Wu, G. Zheng, and G. Hao, "Efficient spatial compliance analysis of general initially curved beams for mechanism synthesis and optimization," *Mechanism and Machine Theory*, vol. 162, 8 2021.

[25] V. K. Venkiteswaran and H.-J. Su, "A Versatile 3R Pseudo-Rigid-Body Model for Initially Curved and Straight Compliant Beams of Uniform Cross Section," *Journal of Mechanical Design*, vol. 140, no. 9, 09 2018.

[26] M. Jafari and M. J. Mahjoob, "An exact three-dimensional beam element with nonuniform cross section," *Journal of Applied Mechanics, Transactions ASME*, vol. 77, 2010.

Chapter 2

Paper II: A validation of a parametric compliance matrix for circularly curved leaf flexures and its application in parallel mechanisms

A validation of a parametric compliance matrix for circularly curved leaf flexures and its application in parallel mechanisms

H.G. Miltenburg

20/09/2023

Abstract

This paper presents a validation of a parametric compliance matrix of a circularly curved leaf flexure (CCLF), which has been obtained using the direct method. This is done for three case studies. In case study one, the compliance matrix of a single flexure is evaluated. The results are compared with the results from a finite element analysis over a range of geometrical parameters. This maps how the geometry of the flexure affects the accuracy of the compliance matrix. It is shown that an increase of both the sweep angle and the height of the flexure show a decrease in the accuracy. Additionally a test setup was built to measure the stiffness of a single flexure to validate the compliance matrix. Furthermore, in case study two and three, the compliance matrices of mechanisms containing multiple flexures in series and parallel are derived with the compliance matrix method, using adjoint transformation matrices. The results are validated by comparison with FEA and measurements from a test setup. A parallel combination of flexures show a decrease in error, when compared to a single flexure.

1 Introduction

In compliant mechanisms motion is achieved by elastic deformation concentrated in parts that are more compliant than the rest of the mechanism. Leaf flexures are commonly used as a compliant element in such mechanisms. In most cases these are initially straight, also known as initially straight leaf flexures (ISLF). To a lesser extent, leaf flexures exist that have a curved geometry before undergoing deformation, called initially curved leaf flexures (ICLF). These curves come in various shapes and are used for different reasons. One motivation to use ICLF is its geometry. Where ISLF always have the same shape, ICLF allow the designer to choose a shape to fit the geometrical constraints of a design. The use of ICLF also allows for cylindrical mechanisms, which have several advantages [1]. Manufacturing cost and time can be reduced since the mechanisms can be made from precision round stock. Axial symmetry allows thermal insensitivity, and an overall reduction in parasitic motions. Several linear guides with a cylindrical shape have been proposed [2] [3] [4], that show a reduction in footprint to range of motion (ROM) ratio. Also, by using elliptical flexures, a cylindrical revolute joint has been proposed, that allows for cables to pass through its center, and would be beneficial in minimal invasive surgery due to its smaller footprint to ROM ratio [5]. In planar mechanisms, ICLF have been used as revolute joints. An initial curvature shows an increase in ROM [6], and a decrease in axis drift and positioning errors with respect to ISLF in planar revolute joints [7]. Circularly curved leaf flexures (CCLF) are flexures with a circular curve, which exists in a single plane. When deformed out of its plane of curvature, it experiences a torque along its length, which results in a twist giving it an extra parasitic motion with respect to ISLF [1]. This has been applied in a spherical mechanism, which shows to decrease the parasitic motion when compared to similar mechanisms with ISLF [8]. Van Houten [9] shows that using two CCLF instead of two ISLF in parallel results in a rotational mechanism with lower axis drift and a lower maximum stress. The curvature of flexures can also be used to create desired stiffness behavior. Splines were used in a mechanism with a constant output torque for a large input [10], or in a generalized synthesis method to create specific load-displacement curves [11]. Using corrugated CCLF, a mechanism with a quasi-constant output force was created for a large displacement [12]. Lin et al. [13] shows that using curved flexure elements allowed for the creation of a relatively simple mechanism with six degrees of freedom (DOF). Several methods have been proposed for modeling the initially curved flexures. For planar mechanisms a pseudo rigid body model (PRBM) was introduced [14] [15], and Chen [16] introduced a beam constrained model (BCM) that is able to capture non-linearities. A compliance matrix is able to capture the linear stiffness of ICLF, for both planar and spatial mechanisms. Jafari and Mahjoob [17]

present a method that is able to obtain compliance matrix of beams with a curved shape, which Parvari Rad et al. applied on a circularly curved leaf flexure [8].

ICLF show certain benefits, when applied correctly. However, few applications exist in the literature, as there are only few models available. FEA is the dominant method used in analysis and synthesis, which gives little to no transparency on the parameters. Additionally, both BCM and PRBM are only applicable to planar mechanisms, and therefore does not support deflections out of the plane of motion. The compliance matrix is able to describe the stiffness in both planar and out of plane motions, and has been applied on a CCLF using the direct method. However, the geometry of a CCLF can take many forms, with different degrees of curvature. It has not been specified for what range of geometries the compliance matrix is accurate, and therefore can be applied. In this paper, a parametric compliance matrix of a CCLF will be derived using the direct method. A parametric evaluation will be done, with the aim to identify how the accuracy of the compliance matrix is affected by the geometry, and to provide geometrical bounds for the model. The model will also be validated using FEA and with an experimental test setup. Also, the compliance matrix of two mechanisms containing multiple CCLF in series and parallel will be derived and validated.

In section 2 the compliance matrix of a single flexure will be derived according to the direct method. It is shown how a compliance matrix of a parallel or serial mechanism can be obtained, using the adjoint transformation matrix. In section 3, the model is validated for three different cases. subsection 3.1 discusses case one, where a single flexure will be validated over a range of parameters to identify how the accuracy of the compliance matrix is affected by the geometry. In case two (subsection 3.2) the compliance matrix will be validated for a parallel mechanism with two CCLF usinf FEA and an experimental test setup. Subsection 3.3 shows the validation of the model using FEA for a parallel mechanism consisting of three legs with each two CCLF in series.

2 Analytical model

2.1 Deriving a compliance matrix for a single CCLF

The compliance matrix of a circular curved leaf flexure (CCLF) has been obtained through the direct method as presented by Jafari and Mahjoob [17]. Consider a CCLF as depicted in Figure 1, with a uniform cross section, width w, and height h. The shape of the CCLF is determined by its centroidal curve with radius R and sweep angle ϕ. The CCLF has a fixed end (left) and a free end. A global coordinate system xyz is located at the free end, with its origin at the end of the centroidal curve.

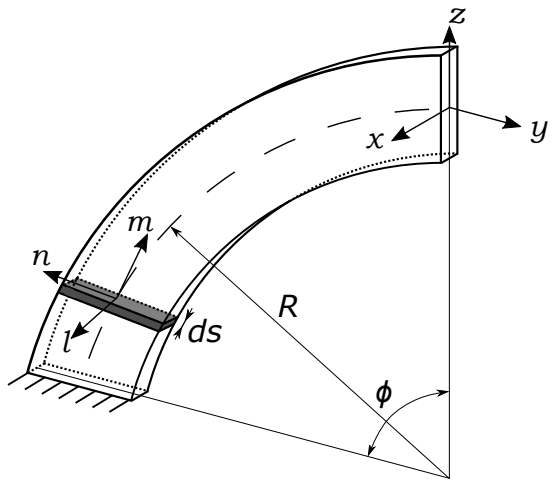

Figure 1: CCLF with coordinate system xyz at the free end, and lmn at element ds.

Loads that are applied at the origin of xyz result in a displacement. The loads and displacements are expressed in the global coordinate system xyz, and are described in load vector f and displacement vector u respectively.

$$\boldsymbol{f} = \begin{bmatrix} f_x & f_y & f_z & m_x & m_y & m_z \end{bmatrix}^T$$
$$\boldsymbol{u} = \begin{bmatrix} \delta_x & \delta_y & \delta_z & \theta_x & \theta_y & \theta_z \end{bmatrix}^T$$

Here, f_x, f_y, and f_z represent the forces and m_x, m_y, and m_z represent the moments at the free end. δ_x, δ_y, δ_z, θ_x, θ_y, and θ_z are the displacements and the rotations along the x, y, and z-axes respectively. The coordinates of the curve through the centroid of the CCLF are described in vector $\boldsymbol{r}(\phi)$ with its components expressed in xyz. A local coordinate system lmn exists for every generic coordinate and accompanying cross section along the curve. Its l-axis lays parallel with the x-axis of xyz, the m-axis lays perpendicular to the cross section, and the n-axis follows the right hand rule. The origin of lmn lays in the center of the cross section, and thus on the centroidal curve. Rotation matrix $\boldsymbol{T}$ expresses the relative orientation between the local and the global coordinate system, such that $[xyz]^T = \boldsymbol{T}[lmn]^T$.

$$\boldsymbol{r}(\phi) = \begin{bmatrix} r_x \\ r_y \\ r_z \end{bmatrix} = \begin{bmatrix} 0 \\ -R\sin(\phi) \\ -R + R\cos(\phi) \end{bmatrix}$$

$$\boldsymbol{T} = \begin{bmatrix} 1 & 0 & 0 \\ 0 & \cos(\phi) & -\sin(\phi) \\ 0 & \sin(\phi) & \cos(\phi) \end{bmatrix}$$

As the free end is externally loaded by load vector $\boldsymbol{f}$, a load is developed at element ds, described in load vector $\boldsymbol{f'}$, which is expressed in local coordinate system lmn.

$$\boldsymbol{f'} = \begin{bmatrix} f_l & f_m & f_n & m_l & m_m & m_n \end{bmatrix}^T \tag{1}$$

The relation between $\boldsymbol{f}$ and $\boldsymbol{f'}$ is as follows

$$\boldsymbol{f'} = \boldsymbol{B}\boldsymbol{f}$$

$$\boldsymbol{B} = \begin{bmatrix} \boldsymbol{T}^T & 0 \\ \boldsymbol{T}^T(\boldsymbol{D}^T) & \boldsymbol{T}^T \end{bmatrix}$$

Here $\boldsymbol{D}$ is the cross-product matrix of vector $\boldsymbol{r}(\phi)$. Due to this load vector $\boldsymbol{f'}$, the element experiences a deformation per unit length as described in $\boldsymbol{\varepsilon}$. These deformations of unit length are related to the load vector by the rigidity matrix ($\boldsymbol{\xi}$) of element ds.

$$\boldsymbol{f'} = \boldsymbol{\xi}\boldsymbol{\varepsilon} \tag{2}$$

$$\boldsymbol{\varepsilon} = \begin{bmatrix} \gamma_{lm} & \epsilon_{mm} & \gamma_{mn} & \kappa_{lm} & \kappa_{mm} & \kappa_{mn} \end{bmatrix}^T$$

$$\boldsymbol{\xi} = \begin{bmatrix} \beta_l GA & 0 & 0 & 0 & 0 & 0 \\ 0 & EA & 0 & 0 & 0 & 0 \\ 0 & 0 & \beta_n GA & 0 & 0 & 0 \\ 0 & 0 & 0 & EI_l & 0 & 0 \\ 0 & 0 & 0 & 0 & GJ & 0 \\ 0 & 0 & 0 & 0 & 0 & EI_n \end{bmatrix}$$

Here, A, I_l, I_n, J, E, G, and β_l and β_n are the cross section area, the area moments of inertia, the torsion constant, the Young's modulus, the shear modulus and the shear coefficients respectively. Multiplying the unit length deformations of the element with its length, gives the deformations of element ds in its local coordinate frame.

$$\mathrm{d}\boldsymbol{u'} = \boldsymbol{\varepsilon}\mathrm{d}s = \boldsymbol{\varepsilon}R\mathrm{d}\phi \tag{3}$$

$$\boldsymbol{u'} = \begin{bmatrix} \delta_l & \delta_m & \delta_n & \theta_l & \theta_m & \theta_n \end{bmatrix}$$

The deformations of the free end relate to the deformations of element ds as follows

$$\mathrm{d}\boldsymbol{u} = \boldsymbol{B}^T\mathrm{d}\boldsymbol{u'} \tag{4}$$

Substituting Equation 1, 2, and 3 into Equation 4 gives

$$\begin{aligned} \mathrm{d}\boldsymbol{u} &= \boldsymbol{B}^T\boldsymbol{\xi}^{-1}\boldsymbol{B}R\boldsymbol{f}\mathrm{d}\phi \\ \boldsymbol{u} &= \int_0^\phi \boldsymbol{B}^T\boldsymbol{\xi}^{-1}\boldsymbol{B}R\mathrm{d}\phi \cdot \boldsymbol{f} \\ \boldsymbol{u} &= \boldsymbol{C}\boldsymbol{f} \\ \boldsymbol{C} &= \int_0^\phi \boldsymbol{B}^T\boldsymbol{\xi}^{-1}\boldsymbol{B}R\mathrm{d}\phi \end{aligned} \tag{5}$$

The integral results in a 6x6 compliance matrix $\boldsymbol{C}$ that shows the relation between $\boldsymbol{u}$ and $\boldsymbol{f}$ at the origin of xyz. The compliance matrix is symmetric and consists of 18 nonzero elements. These elements are written as $C_{i,j}$. Each element describes the relation between a certain displacement (i), and load (j). Since the matrix is symmetric, 12 out of 18 elements are independent.

$$\boldsymbol{C} = \begin{bmatrix} C_{x,f_x} & 0 & 0 & 0 & C_{x,m_y} & C_{x,m_z} \\ 0 & C_{y,f_y} & C_{y,f_z} & C_{y,m_x} & 0 & 0 \\ 0 & C_{z,f_y} & C_{z,f_z} & C_{z,m_x} & 0 & 0 \\ 0 & C_{r_x,f_y} & C_{r_x,f_z} & C_{r_x,m_x} & 0 & 0 \\ C_{r_y,f_x} & 0 & 0 & 0 & C_{r_y,m_y} & C_{r_y,m_z} \\ C_{r_z,f_x} & 0 & 0 & 0 & C_{r_z,m_y} & C_{r_z,m_z} \end{bmatrix}$$

The stiffness matrix can be obtained by taking the inverse of the compliance matrix.

$$\boldsymbol{K} = \boldsymbol{C}^{-1}$$

$$\boldsymbol{K} = \begin{bmatrix} K_{f_x,x} & 0 & 0 & 0 & K_{F_x,r_y} & K_{f_x,r_z} \\ 0 & K_{f_y,y} & K_{F_y,z} & K_{f_y,r_x} & 0 & 0 \\ 0 & K_{f_z,y} & K_{F_z,z} & K_{f_z,r_x} & 0 & 0 \\ 0 & K_{m_x,y} & K_{m_x,z} & K_{m_x,r_x} & 0 & 0 \\ K_{m_y,x} & 0 & 0 & 0 & K_{m_y,r_y} & C_{m_y,r_z} \\ K_{m_z,x} & 0 & 0 & 0 & K_{m_z,r_y} & C_{m_z,r_z} \end{bmatrix}$$

Through this method, the compliance matrix is obtained by taking the integral over dϕ. The compliance matrix as shown in Equation 5 contains definite integrals over dϕ with an interval of $[0, \phi]$. Integrating over this interval results in a compliance matrix with elements that are closed form parametric expressions. These expressions can be found in Appendix A.

2.2 Transformation and combination of compliance matrices in parallel and serial mechanisms

The compliance matrix from the previous section describes the behavior of a single flexure, in a coordinate system that coincides with the free end. In serial and parallel mechanisms, the base and the EE are connected by multiple flexure elements. The compliance matrix of such mechanisms can be obtained with the compliance matrix method [18]. This method states that flexure elements can be transformed from their local coordinate systems to a defined global coordinate system, after which the compliance matrices can be added for serial mechanisms, and the stiffness matrices can be added for parallel mechanisms. The transformation of flexure i from the local to the global coordinate system consists of a rotation and a translation, and can be achieved using the adjoint transformation matrix $\boldsymbol{Ad}_i$ [19]. $\boldsymbol{T}_i$ shows the rotation matrix, and $\boldsymbol{S}_i$ is the cross product matrix of translation vector $\boldsymbol{s}_i$ from the local to the global coordinate system. $\boldsymbol{s}_i$ is expressed in the global coordinate system.

$$\boldsymbol{C}_{global,i} = \boldsymbol{Ad}_i \boldsymbol{C}_{local,i} \boldsymbol{Ad}_i^T$$

$$\boldsymbol{Ad}_i = \begin{bmatrix} \boldsymbol{T}_i & \boldsymbol{S}_i^T \boldsymbol{T}_i \\ 0 & \boldsymbol{T}_i \end{bmatrix}$$

$$\boldsymbol{S}_i = \begin{bmatrix} 0 & -\boldsymbol{s}_{Z,i} & \boldsymbol{s}_{Y,i} \\ \boldsymbol{s}_{Z,i} & 0 & -\boldsymbol{s}_{X,i} \\ -\boldsymbol{s}_{Y,i} & \boldsymbol{s}_{X,i} & 0 \end{bmatrix}$$

For a serial chain of flexure elements, the compliance matrices can be added as follows

$$\boldsymbol{C}_{total} = \sum_{i=1}^{n} \boldsymbol{C}_{global,i} \qquad \boldsymbol{K}_{total} = \left(\sum_{i=1}^{n} \frac{1}{\boldsymbol{K}_{global,i}} \right)^{-1}$$

For parallel flexure elements the following rules apply

$$\boldsymbol{C}_{total} = \left(\sum_{i=1}^{n} \frac{1}{\boldsymbol{C}_{global,i}} \right)^{-1} \qquad \boldsymbol{K}_{total} = \sum_{i=1}^{n} \boldsymbol{K}_{global,i}$$

3 Validation

The analytical model is validated through comparison with results from a finite element analysis (FEA), and the results from an experimental test setup. This is done for three case studies. In case study one the accuracy of a single flexure is analyzed over a range of geometries, to identify which geometrical parameters affect the accuracy and to what extent. A single geometry is also tested in an experimental test setup. Case study two will investigate a parallel mechanism, existing of two identical flexures to verify the accuracy of the model for flexures in parallel. The third case study concerns a mechanism that contains six CCLF. It shows whether the model can be used in complex spatial mechanisms containing multiple flexures both in series and parallel.

3.1 Case study 1: A single flexure

3.1.1 Validation over range of parameters using FEA

As the geometry of a curved flexure will change by varying the geometrical parameters, an infinite range of curved flexures can be formed. In order to asses which of these parameters affect the accuracy, an evaluation of the accuracy of the model with respect to FEA will be done over a range of selected parameters. The curvature of the flexure is described by the sweep angle for a constant L, since $L = R\phi$ as it concerns CCLF. Figure 2 shows how the curvature changes for changing ϕ. In this evaluation, the length is constant at $L = 150\,\text{mm}$, and the sweep angle will increase over $\phi = [1°, 30°, 60°, 90°, 120°, 150°, 180°]$. $\phi = 1°$ is chosen to approach an

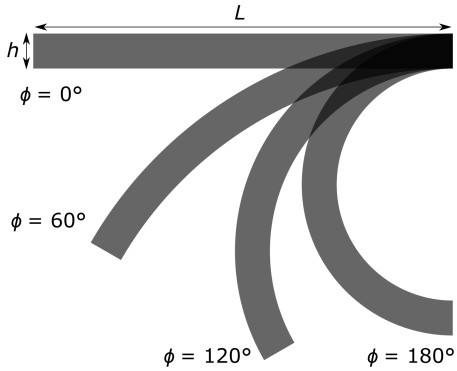

Figure 2: For a constant length L, an increasing sweep angle ϕ results in a decrease of radius R.

ISLF. A second parameter of interest is the height, which is described as ratio L/h, in order to make it dimensionless. The ratio will be evaluated over $L/h = [7.5, 10, 12.5, 15]$. The influence of the width w of the flexure is not considered for now and is held constant with respect to the height as $w = h/10$. The material used in this validation is steel, with a Young's modulus $E = 200\,\text{GPa}$ and Poisson's ratio $\nu = 0.3$. For rectangular cross sections, the shear coefficient is $\beta_l = \beta_n = \frac{10(1+\nu)}{12+11\nu} = 0.850$ [20].

For the FEA, *Ansys* software is used. Since the analytical model does not consider non-linearities, linear analysis is used. The mesh consists of second order mesh elements with a rectangular shape. For every geometry, a convergence study has been conducted to validate the FEA results. Mesh refinements are done until the result does not vary more than 1 % with respect to the previous mesh. When this occurs in two successive mesh refinements, convergence is considered. For each geometry that has been specified, the six diagonal elements of the stiffness matrix are obtained with the analytical model and the FEA. The percentage error between the results are plotted as a function of ϕ in Figure 3. The color of the plot indicates the ratio L/h.

3.1.2 Experimental test setup

To further validate the model for a single flexure, an experimental test setup is built. A flexure with $L = 120\,\text{mm}$, $\phi = 90°$, and $h = 12\,\text{mm}$ was laser-cut from a 1 mm thick stainless steel plate. with $E = 193\,\text{GPa}$ and $\nu = 0.31$. One end was fixed, while the other end is attached to an aluminium end effector(EE). The EE can be constrained using a linear or rotary bearing, such that only a single motion is allowed. The direction of this allowable motion is determined by the orientation of the bearing on the EE. The stiffness of the flexure can be measured in the direction of the allowable motion. This is done by

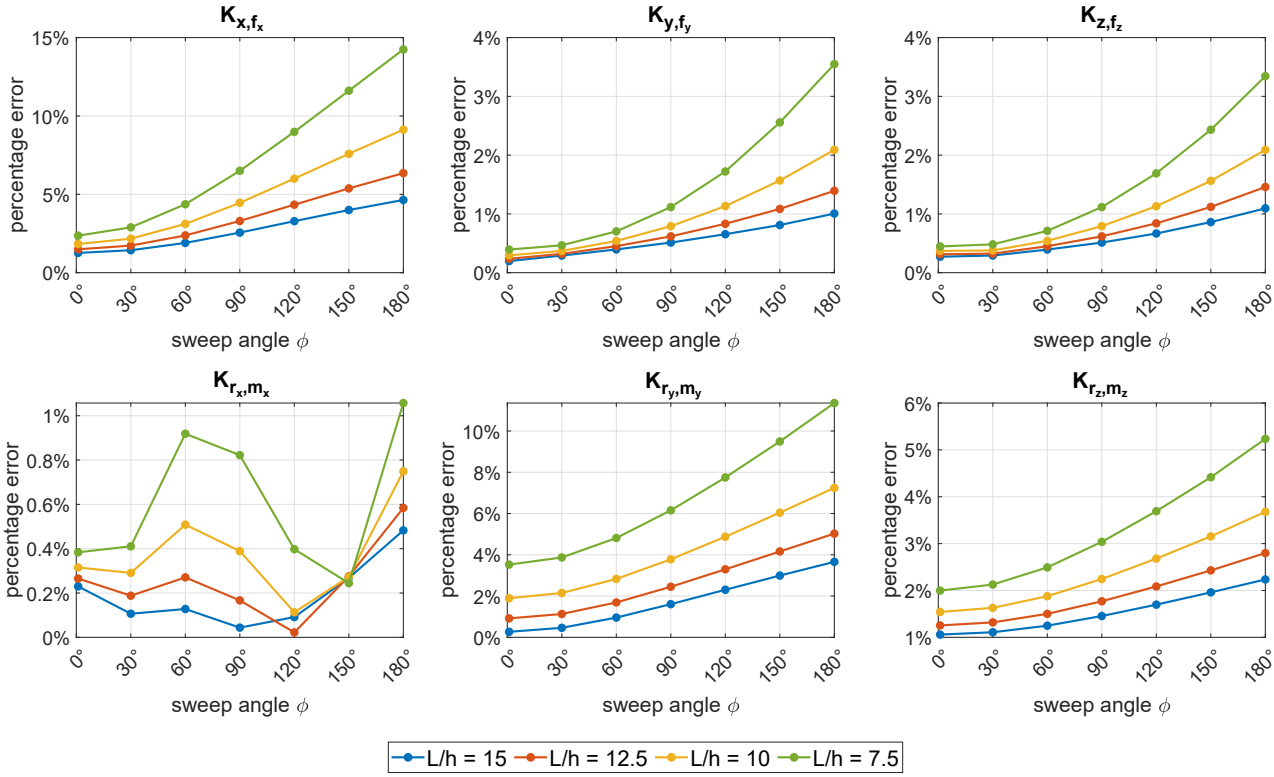

Figure 3: The error percentages of the analytical model when compared to FEA for a range of parameters.

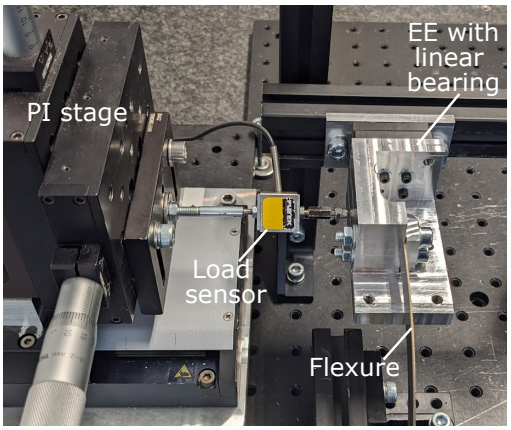

Figure 4: The experimental test setup with a linear bearing attached to the EE for measuring K_{x,f_x}.

a load sensor which is attached to a linear PI stage. A displacement of the EE can be achieved by the PI stage, which results in a deflection of the flexure. The load sensor measures the needed load for the deflection. For rotations, a lever is attached to the EE such that a linear motion can cause a small rotation of the EE. Figure 4 and Figure 5 show the test setup for stiffness elements K_{x,f_x} and K_{r_y,m_y} respectively.

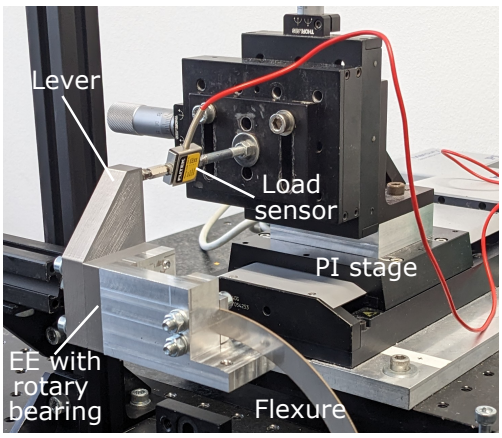

Figure 5: The experimental test setup with a rotary bearing attached to the EE for measuring K_{r_y,m_y}.

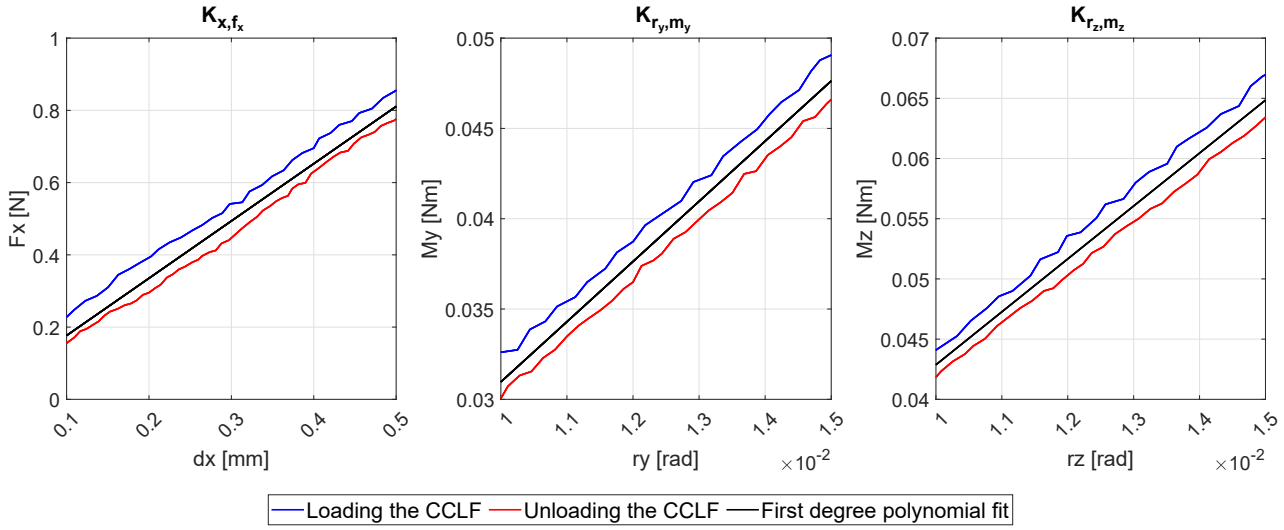

Figure 6: Results from the test setup for the translational stiffness in x, the rotational stiffness around y, and the rotational stiffness around z respectively, for a single CCLF.

The experimental test setup was used to measure the stiffness of the three DOF of the flexure. The PI stage is able to move with a resolution of ≈ 0.01 mm, which is too large for measuring the elastic regime of the stiffness in the DOC. Figure 6 shows the load-deflection curve for the three measured directions. The plots are magnified to show the data for the linear regime. A first degree polynomial was fitted on the shown data, which gives the linear stiffness. Table 1 show the results from the analytical model, compared to the results from FEA and the test setup, with their respective error percentages.

Table 1: Comparisson of the results from the analytical model, FEA, and the test setup, with their respective percentage error for a single CCLF.

	Analytical model	**FEA**	**Error** [%]	**Test setup**	**Error** [%]
K_{x,f_x} [N/m]	1.59e3	1.68e3	5.40	1.59e3	4.43e-1
K_{y,f_y} [N/m]	1.98e6	2.01e6	1.12	-	-
K_{z,f_z} [N/m]	1.98e6	2.01e6	1.12	-	-
K_{r_x,m_x} [Nm/rad]	1.67e3	1.67e3	1.82e-1	-	-
K_{r_y,m_y} [Nm/rad]	3.50	3.72	5.87	3.33	4.98
K_{r_z,m_z} [Nm/rad]	5.15	5.28	2.52	4.40	1.72e1

3.2 Case study 2: rotational DOF parallel mechanism

For case study two, the accuracy of the analytically obtained results will be analyzed for a parallel mechanism. Two circularly curved flexures are placed under an angle $\theta = 60\,^\circ$ around the Z-axis of the global coordinate system XYZ, such that both flexures have a rotational offset of $\theta/2$ from the YZ-plane. The free ends of the flexures are both positioned

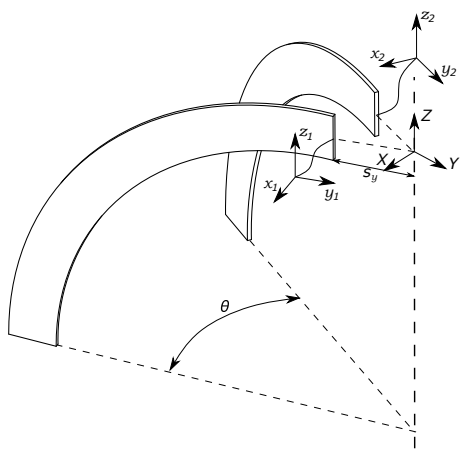

Figure 7: The parallel mechanism of case study two.

a distance $s_y = 21.05$ mm from the global coordinate system, as is shown in Figure 7. The flexures have the same dimensions and material properties as the single flexure in case study one (subsection 3.1). Since the constraints of a parallel mechanism are determined by the span of constraints of the single flexure elements, the mechanism has a single rotational DOF around Z.

3.2.1 FEA

For the FEA, the same settings are used as for the single CCLF in subsection 3.1. The free end of both flexures were rigidly connected to the global coordinate system. To ensure the validity of the results, a mesh convergence study was carried out. The FEA results are presented in Table 2.

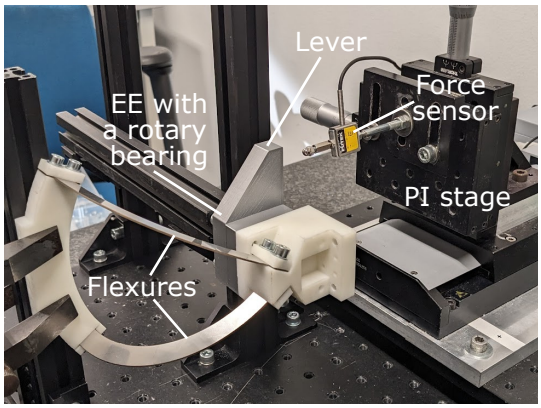

Figure 8: The experimental test setup for the parallel mechanism.

Table 2: Comparison of the results from the analytical model, FEA, and the test setup, with their respective percentage error for a parallel mechanism with one rotational DOF.

	Analytical model	**FEA**	**Error** [%]	**Test setup**	**Error** [%]
K_{x,f_x} [N/m]	9.94e5	1.01e6	1.12	-	-
K_{y,f_y} [N/m]	2.97e6	3.01e6	1.11	-	-
K_{z,f_z} [N/m]	3.97e6	4.01e6	1.10	-	-
K_{r_x,m_x} [Nm/rad]	6.81e3	6.82e3	2.11e-1	-	-
K_{r_y,m_y} [Nm/rad]	2.27e3	2.28e3	2.23e-1	-	-
K_{r_z,m_z} [Nm/rad]	1.77e1	1.83e1	3.22	1.59e1	1.16e1

3.2.2 Test setup

In order to measure the stiffness in a test setup, the mechanism has been built using flexures that were laser-cut from a plate of stainless steel. The same material properties as in subsection 3.1 apply. The EE has been fabricated using a resin printer with *Formlabs RIGID 10K* resin, which has a Young's modulus $E = 10\,\text{GPa}$. Similarly to the test setup in subsection 3.1, the EE is connected to a bearing such that the axis of rotation of the mechanism coincides with the axis of rotation of the bearing, in order to isolate its DOF. The moment is plotted against the rotation of the EE in Figure 9. The black line shows a first degree polynomial fit over the shown data, where the deflections are sufficiently small to be considered linear. The measured stiffness is found in Table 2.

3.3 Case study 3: Three legged parallel mechanism

For case study three, the model of a mechanism with both flexures in series, aswell as in parallel will be validated. The mechanism (Figure 10) consists of three legs in parallel, where each leg contains two identical flexure elements in series. In each leg, the flexure elements are connected by an intermediate body with a length of 20 mm, and are orientated under an angle $\beta = 120\,°$. The three legs are positioned around the Z-axis of the global coordinate system XYZ with circular symmetry and equal spacing. The legs are positioned with a distance of $S_X = 20\,\text{mm}$ in the XY-plane from the origin of XYZ.

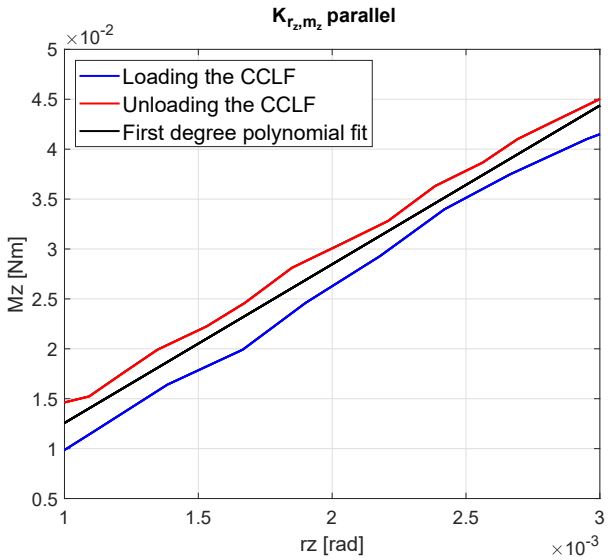

Figure 9: Results from the test setup for the rotational stiffness around z for the parallel mechanism.

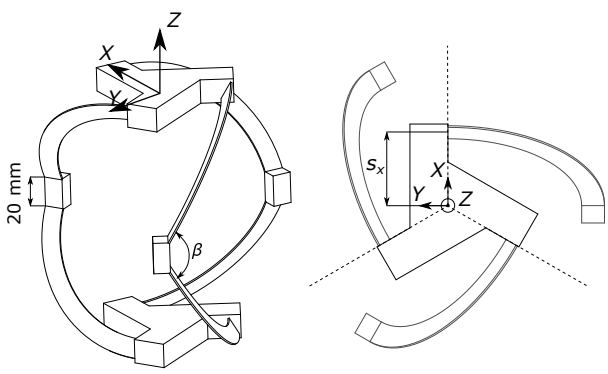

Figure 10: The parallel mechanism containing three legs in parallel, each containing 2 CCLF in series (left), and the top view of the mechanism (right).

The stiffness of the mechanism in the global coordinate system has been obtained with the analytical method, and a linear FEA. The FEA used the same settings as discussed in subsection 3.1. To link the two flexure elements in each leg, an intermediate body was used, which was given a Young's modulus with a magnitude 10^5 higher than the flexures.

This way, its contribution to the stiffness can be neglected, as is desired, since the analytical model considers these intermediate bodies as rigid. The results are presented and compared in Table 3.

Table 3: Comparison of the results from the analytical model and FEA, with their respective percentage error for the three legged parallel mechanism.

	Analytical model	**FEA**	**Error** [%]
K_{x,f_x} [N/m]	4.19e4	4.22e4	6.02e-1
K_{y,f_y} [N/m]	4.19e4	4.22e4	6.02e-1
K_{z,f_z} [N/m]	9.44e3	9.97e3	5.34
K_{r_x,m_x} [Nm/rad]	2.60e2	2.62e2	7.25e-1
K_{r_y,m_y} [Nm/rad]	2.60e2	2.62e2	7.25e-1
K_{r_z,m_z} [Nm/rad]	5.15e1	5.18e1	6.75e-1

4 Discussion

In section 3, three case studies were carried out to validate the compliance matrix obtained with the direct method. For a single flexuere, a study has been done to see what impact the height h and sweep angle ϕ have on the accuracy of the model. The percentage error increases for an increase in both ϕ and h, as shown in Figure 3. This can be attributed to the neglect of the inner and outer radius of the flexure in the model, as the direct method integrates the unitless deformations over the centroidal curve. Therefore no distinction is made in the difference of R_i and R_o. The relative difference between the inner and outer radius can be expressed as h/R. Both for an increase in ϕ and h, this relative difference will increase. When it increases, the difference becomes more dominant and neglecting it results in an increase of percentage error. Therefore, the geometries with a low ϕ or a high L/h show lower percentage errors. To stay under 5 % error, a ratio $L/h \geq 15$ should be maintained for flexures with a sweep angle of 180 °. For a flexure with a ratio $L/h = 10$, the error is ≤ 5 % for a sweep angle up to 100 °. In Table 1, the results from the model, the linear FEA, and the test setup are compared. It shows that the FEA results are higher, whereas the stiffnesses measured in the test setup are lower than the stiffnesses from the analytical model. The FEA results tend to be higher, because it takes the difference between the inner and outer radius into account, unlike the compliance matrix. The lower stiffnesses from the test setup can be explained as the test setup does not only measure the deflection of the flexure, but also all other objects present between the PI stage and the fixed end of the flexure. Since these objects create a serial linkage, the deflections add up, resulting in a lower overall measured stiffness. To minimize this, effort was made to include objects with higher stiffness than the stiffness of the flexure in the direction of interest. This applies especially where high stresses are expected, such as the connections of the flexure to the EE and the fixed end. The offset between the loading curve and the unloading curve of the experimental setup can be explained by hysteresis created the friction in the bearings.

In case study two, two flexures are combined in parallel. The compliance matrix of the mechanism is obtained analytically, and has been validated with FEA and a test setup. The results in Table 2 show lower percentage error with respect to the results of the single flexure in case one. By combining flexures in parallel, its parasitic motions are constrained. The absence of the parasitic motions may cause the reduction in percentage error of the parallel mechanism. The mechanism of case study three, has been validated with FEA. Table 3 shows that the analytical model is able to capture the stiffnesses of a complex spatial mechanism with a maximum error of 5.34 %.

This study is done to see to how the accuracy of the model is affected by the degree of curvature. Since the width w is not in the plane of curvature considered in this study, it is left out and held constant as $w = h/10$. However, it might be worth to include this parameter in a future study, since it does have an affect on both area moments of inertia I_l, and I_m, and therefore might provide further insight on the affecting parameters. With the knowledge from this paper, one could investigate how the model could be improved, for example by including the difference of inner and outer radius.

The flexures discussed in this paper have a constant cross section area along its length and have a circular shape in a single plane. Many different shapes of curvature exist, such as splines and Bézier curves, but also spatial curves like a spiral and a helix. The direct method allows to be applied on beams with any curve that can be described mathematically and also allow a change of cross section along the length of the flexure. Future research would involve the application and validation of the direct method on different shapes, but also on flexures with varying cross section areas.

5 Conclusion

This paper presents a parametric compliance matrix of a single flexure with a circular curvature using the direct method. A validation has been done for a

range of geometrical parameters, to understand how they affect the accuracy of the model. For a single flexure with a constant length and width, both an increase in height and sweep angle give an increase of the percentage error of the model. This has been attributed to the neglect of the inner and outer radius during the derivation of the compliance matrix using the direct method. During application of the direct method, one should therefore consider the trade-off between a large ϕ and a low L/h when a certain accuracy is required. As a reference, an error $\leq$4.64 % is achieved for $L/h = 15$ up to a sweep angle $\phi = 180°$. Decreasing L/h or increasing ϕ would lead to a lower accuracy.

A parametric compliance matrix of a mechanism consisting of multiple CCLF in series or parallel can be obtained using matrix transformation of the individual flexure elements. For the parallel mechanism containing two CCLF discussed in this paper, an increase of accuracy is observed with respect to the compliance matrix of a single CCLF. The two parallel mechanisms that were evaluated in this paper showed a maximum error of 5.34 %, when compared to FEA. This makes the model a versatile tool for analysis of mechanisms containing multiple flexures in series and parallel. The parametric nature of the model also makes it evident to perform parametric optimizations.

References

[1] M. J. Telleria and M. L. Culpepper, "Understanding the drivers for the development of design rules for the synthesis of cylindrical flexures," *Mechanical Sciences*, vol. 3, pp. 25–32, 2012.

[2] M. J. Telleria, "Design rules and models for the synthesis and optimization of cylindrical flexures," Ph.D. dissertation, Massachusetts Institute of Technology, 2013.

[3] M. Yang, C. Zhang, X. Huang, S. L. Chen, and G. Yang, "A long stroke nanopositioning stage with annular flexure guides," *IEEE/ASME Transactions on Mechatronics*, vol. 27, pp. 1570–1581, 6 2021.

[4] T. Liu and G. Hao, "Design of a cylindrical compliant linear guide with decoupling parallelogram mechanisms," *Micromachines*, vol. 13, no. 8, 2022. [Online]. Available: https://www.mdpi.com/2072-666X/13/8/1275

[5] J. Dearden, C. Grames, J. Orr, B. D. Jensen, S. P. Magleby, and L. L. Howell, "Cylindrical cross-axis flexural pivots," *Precision Engineering*, vol. 51, pp. 604–613, 1 2018.

[6] G. Berselli, F. Parvari Rad, R. Vertechy, and V. Parenti Castelli, "Comparative evaluation of straight and curved beam flexures for selectively compliant mechanisms," in *2013 IEEE/ASME International Conference on Advanced Intelligent Mechatronics*, 2013, pp. 1761–1766.

[7] M. Verotti, "Effect of initial curvature in uniform flexures on position accuracy," *Mechanism and Machine Theory*, vol. 119, pp. 106–118, 2018. [Online]. Available: https://www.sciencedirect.com/science/article/pii/S0094114X17309059

[8] F. Parvari Rad, G. Berselli, R. Vertechy, and V. Parenti-Castelli, "Design and stiffness analysis of a compliant spherical chain with three degrees of freedom," *Precision Engineering*, vol. 47, pp. 1–9, 2017. [Online]. Available: https://www.sciencedirect.com/science/article/pii/S0141635916300897

[9] A. Van Houten, "Rcm mechanism based on curved flexures," Master's thesis, TU DELFT, the Netherlands, 2021.

[10] H. N. Prakashah and H. Zhou, "Synthesis of constant torque compliant mechanisms," *Journal of Mechanisms and Robotics*, vol. 8, 12 2016.

[11] C. V. Jutte and S. Kota, "Design of nonlinear springs for prescribed load-displacement functions," vol. 130, 8 2008, pp. 0 814 031–08 140 310.

[12] Q. Zhang, P. Yan, and H. Wang, "A curved-beam based quasi-constant force mechanism supporting large range and force-sensitive robotic manipulation," *Mechanism and Machine Theory*, vol. 172, p. 104799, 6 2022.

[13] S. Lin, J. Wang, W. Xiong, Q. Hu, H. Liu, and Q. Wang, "Design and modeling of a curved beam compliant mechanism with six degrees of freedom," *Micromachines*, vol. 13, no. 2, 2022. [Online]. Available: https://www.mdpi.com/2072-666X/13/2/208

[14] V. K. Venkiteswaran and H. J. Su, "Pseudo-rigid-body models for circular beams under combined tip loads," *Mechanism and Machine Theory*, vol. 106, pp. 80–93, 12 2016.

[15] V. K. Venkiteswaran and H.-J. Su, "A Versatile 3R Pseudo-Rigid-Body Model for Initially Curved and Straight Compliant Beams of Uniform Cross Section," *Journal of Mechanical Design*, vol. 140, no. 9, 09 2018.

[16] G. Chen, F. Ma, G. Hao, and W. Zhu, "Modeling large deflections of initially curved beams in compliant mechanisms using chained beam constraint model," *Journal of Mechanisms and Robotics*, vol. 11, 2 2019.

[17] M. Jafari and M. J. Mahjoob, "An exact three-dimensional beam element with nonuniform cross section," *Journal of Applied Mechanics, Transactions ASME*, vol. 77, 2010.

[18] M. Arredondo-Soto, E. Cuan-Urquizo, and A. Gómez-Espinosa, "The compliance matrix method for the kinetostatic analysis of flexure-based compliant parallel mechanisms: Conventions and general force–displacement cases," *Mechanism and Machine Theory*, vol. 168, p. 104583, 2022. [Online]. Available: https://www.sciencedirect.com/science/article/pii/S0094114X21003256

[19] H. J. Su, H. Shi, and J. Yu, "A symbolic formulation for analytical compliance analysis and synthesis of

flexure mechanisms," *Journal of Mechanical Design, Transactions of the ASME*, vol. 134, 2012.

[20] G. R. Cowper, "The Shear Coefficient in Timoshenko's Beam Theory," *Journal of Applied Mechanics*, vol. 33, no. 2, pp. 335–340, 06 1966. [Online]. Available: https://doi.org/10.1115/1.3625046

A Parametric compliance matrix

In order to obtain the compliance matrix of a CCLF using the direct method, one needs to integrate over an interval indicating the sweep angle of the flexure. This integration starts at the fixed end (0) upto the free end (ϕ). By executing the integral and substituting 0 and parameter ϕ, the elements are reduced to parametric closed form expressions. Now, the compliance matrix of a geometry can be obtained by substitution of the parameters.

Below, the parametric elements of a compliance matrix for CCLF is shown. Table 4 and 5 show the parameters of the compliance matrix and their relations.

Table 4: List of parameters

Symbol	**Parameter**	**Unit**
ϕ	Sweep angle	[°]
R	Radius	[m]
h	Height	[m]
w	Width	[m]
A	Cross section area	[m^2]
β_n, β_l	Shear coefficients	[-]
J	Torsion constant	[m^4]
I_n, I_l	Area moment of inertia	[m^4]
E	Young's modulus	[Pa]
G	Shear modulus	[Pa]
ν	Poisson's ratio	[-]

Table 5: Relations between parameters

$$R = \frac{L}{\phi}$$
$$I_l = \frac{wh^3}{12}$$
$$I_n = \frac{hw^3}{12}$$
$$G = \frac{E}{2(1+\nu)}$$
$$A = wh$$

$$\boldsymbol{C} = \begin{bmatrix} C_{x,f_x} & 0 & 0 & 0 & C_{x,m_y} & C_{x,m_z} \\ 0 & C_{y,f_y} & C_{y,f_z} & C_{y,m_x} & 0 & 0 \\ 0 & C_{z,f_y} & C_{z,f_z} & C_{z,m_x} & 0 & 0 \\ 0 & C_{r_x,f_y} & C_{r_x,f_z} & C_{r_x,m_x} & 0 & 0 \\ C_{r_y,f_x} & 0 & 0 & 0 & C_{r_y,m_y} & C_{r_y,m_z} \\ C_{r_z,f_x} & 0 & 0 & 0 & C_{r_z,m_y} & C_{r_z,m_z} \end{bmatrix}$$

$$C_{x,f_x} = \frac{R^3\sin(2\phi)}{4GJ} - \frac{R^3\sin(2\phi)}{4EI_n} - \frac{2R^3\sin(\phi)}{GJ} + \frac{R^3\phi}{2EI_n} + \frac{3R^3\phi}{2GJ} + \frac{R\phi}{A\beta_l G}$$

$$C_{y,f_y} = \frac{R(2EI_l\phi - EI_l\sin(2\phi) + \beta_n GI_l\sin(2\phi) + 2\beta_n GI_l\phi + A\beta_n GR^2\sin(2\phi) + 6A\beta_n GR^2\phi - 8A\beta_n GR^2\sin(\phi))}{4A\beta_n EGI_l}$$

$$C_{z,f_z} = \frac{R(EI_l\sin(2\phi) + 2EI_l\phi - \beta_n GI_l\sin(2\phi) + 2\beta_n GI_l\phi - A\beta_n GR^2\sin(2\phi) + 2A\beta_n GR^2\phi)}{4A\beta_n EGI_l}$$

$$C_{r_x,m_x} = \frac{R\phi}{EI_l}$$

$$C_{r_y,m_y} = \frac{R(EI_n\sin(2\phi) - GJ\sin(2\phi) + 2EI_n\phi + 2GJ\phi)}{4EGI_nJ}$$

$$C_{r_z,m_z} = \frac{R(GJ\sin(2\phi) - EI_n\sin(2\phi) + 2EI_n\phi + 2GJ\phi)}{4EGI_nJ}$$

$$C_{r_y,f_x} = C_{x,m_y} = \frac{R^2(EI_n\sin(2\phi) - GJ\sin(2\phi) + 2EI_n\phi + 2GJ\phi - 4EI_n\sin(\phi))}{4EGInJ}$$

$$C_{x,m_z} = C_{r_z,f_x} = -\frac{2R^2}{GJ} - \frac{2R^2(\sin(\phi/2)^2 - 1)(EI_n + EI_n\sin(\phi/2)^2 - GJ\sin(\phi/2)^2)}{EGI_nJ}$$

$$C_{y,f_z} = C_{z,f_y} = \frac{2R\sin(\phi/2)^2(\sin(\phi/2)^2 - 1)}{A\beta_n G} - \frac{2R^3}{EI_l} - \frac{2R(\sin(\phi/2)^2 - 1)(\beta_n I_l\sin(\phi/2)^2 + A\beta_n R^2 + A\beta_n R^2\sin(\phi/2)^2)}{A\beta_n EI_l}$$

$$C_{y,m_x} = C_{r_x,f_y} = \frac{-(R^2(\phi - \sin(\phi)))}{EI_l}$$

$$C_{z,m_x} = C_{r_x,f_z} = \frac{R^2}{EI_l} - \frac{(R^2\cos(\phi))}{EI_l}$$

$$C_{r_y,m_z} = C_{r_z,m_y} = \frac{R(EI_n - GJ)}{4EGI_nJ} - \frac{R\cos(2\phi)(EI_n - GJ)}{4EGI_nJ}$$

B Circularly curved leaf flexures

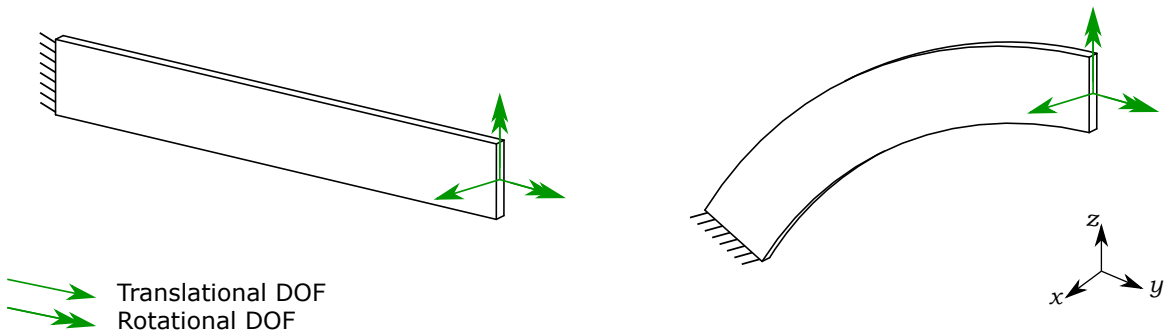

Figure 11: The degrees of freedom of an ISLF(left) and a CCLF(right)

An initially straight leaf flexure (ISLF) has three degrees of freedom (DOF). As depicted in Figure 11, these are a translational DOF in the x direction, a rotational DOF around the y-axis, and a rotational DOF around the z-axis. With the same orientation of its free end, a CCLF has the same DOF as an ISLF. Therefore, an additional DOF or DOC is not achieved by introducing an initial curvature to the leaf flexure. The curvature does however introduce an additional parasitic motion. When an ISLF undergoes a deflection in the x-direction, it experiences a parasitic motion that is a rotation around the z-axis. When a CCLF is actuated by a force in the x-direction, not only does it have a parasitic rotation around z, it also experiences a rotation around the y-axis. Because of the curvature, the force in x creates a torque along the length of the flexure which creates a twisting motion. This results in the additional parasitic rotation around y. This can also be visualised, by comparing a CCLF with two ISLF in series under an angle of 90 °, as shown in Figure 12.

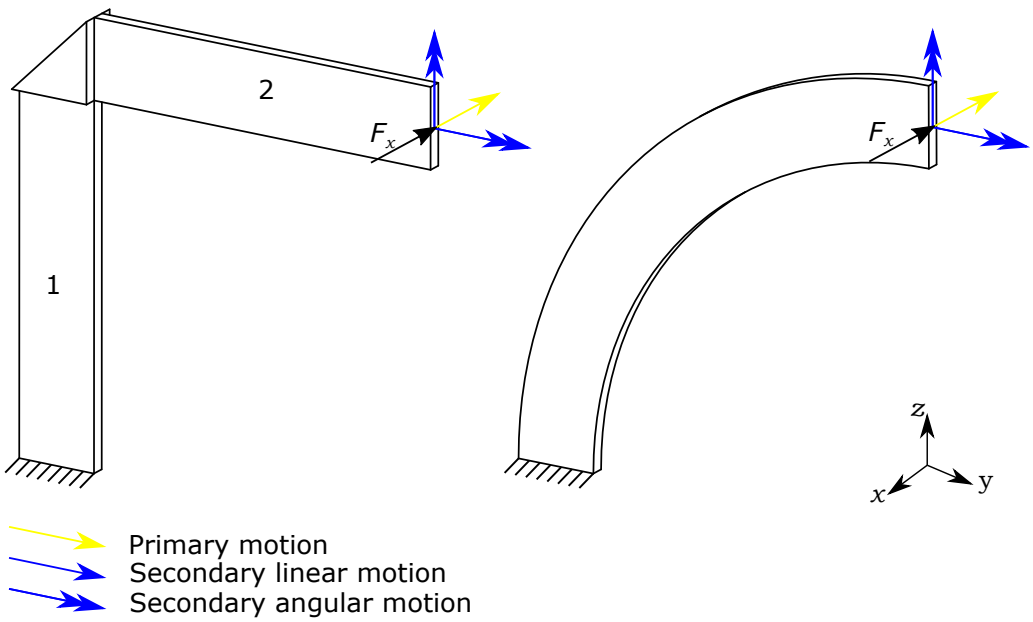

Figure 12: Parasitic motions of two ISLF in series, three ISLF in series, and a CCLF.

In the figure, the yellow arrows represent the primary motions, and the blue arrows represent the secondary, or parasitic motions for small deflections in x. The serial linkage of two ISLF (labeled as flexure 1 and flexure 2) are connected by an intermediate body. Due to its orientation, the bending of flexure 1 results in a parasitic rotation around y, while the bending of flexure 2 results in a parasitic rotation around z. Furthermore, flexure 2 acts as a lever for F_x, creating a Torque around the length of flexure 1, which results in a twist around z. A CCLF can therefore be seen as an exotic variant of two ISLF in series, where the sweep angle of the CCLF determines the angle between the two ISLF in series.

C Derivation of compliance matrix for case study two

A parallel mechanism is formed by combining two CCLF under an angle θ around Z of global coordinate system XYZ, as depicted in Figure 13. A closeup of the local coordinate system at the free end of each flexure element is shown. the y axis of the local coordinate systems meet at a distance $s_y = 21.047\,\text{mm}$ from the free end, which is at the origin of the new global coordinate system XYZ of the parallel mechanism. The constraints of a parallel mechanism are determined by the span of the constraints of each flexure element. Since the individual constraint in y_1 and y_2 are orientated with angle θ from each other, the span covers the entire XY-plane. Both flexure elements also constrain linear motion in Z, making the parallel mechanism constrained for all linear motions. The span of the rotational constraints around x_1 and x_2 result in a rotational constraint around both X as Y, leaving the rotation around Z the only DOF of the formed parallel mechanism.

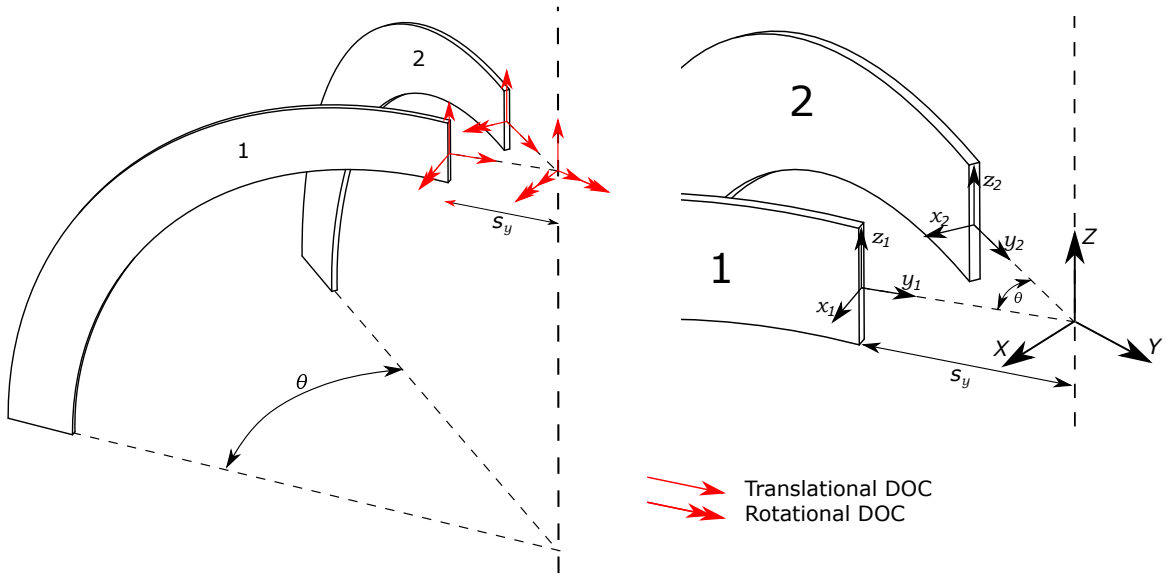

Figure 13: The constraint of the parallel mechanism.

The compliance matrix of the single flexure elements are expressed in each their own local coordinate sytem. To obtain a compiance matrix of the parallel mechanism, expressed in the global coordinate system, the individual compliance matrices of the flexure elements first need to be transformed to the global coordinate system. This can be achieved using the adjoint transformation matrix $\boldsymbol{Ad}$, such that

$$\boldsymbol{C}_{global} = \boldsymbol{Ad}\boldsymbol{C}_{local,i}\boldsymbol{Ad}^T$$

The adjoint transformation matrix transforms the matrix from its local coordinate system to the global coordinate system. The rotations are carried out by rotation matrix $\boldsymbol{T}$ and the translation is done by the cross product matrix $\boldsymbol{S}$ of the translation vector $\boldsymbol{s}$.

$$\boldsymbol{Ad} = \begin{bmatrix} \boldsymbol{T} & \boldsymbol{S}^T\boldsymbol{T} \\ 0 & \boldsymbol{T} \end{bmatrix}$$

$$\boldsymbol{S} = \begin{bmatrix} 0 & -\boldsymbol{s}_Z & \boldsymbol{s}_Y \\ \boldsymbol{s}_Z & 0 & -\boldsymbol{s}_X \\ -\boldsymbol{s}_Y & \boldsymbol{s}_X & 0 \end{bmatrix}$$

For flexure 1 and flexure 2, the rotation matrices $\boldsymbol{T}_1$, and $\boldsymbol{T_2}$ are as follows

$$\boldsymbol{T}_1 = \begin{bmatrix} \cos(\theta/2) & -sin(\theta/2) & 0 \\ \sin(\theta/2) & \cos(\theta/2) & 0 \\ 0 & 0 & 1 \end{bmatrix}, \qquad \boldsymbol{T}_2 = \begin{bmatrix} \cos(\theta/2) & sin(\theta/2) & 0 \\ -\sin(\theta/2) & \cos(\theta/2) & 0 \\ 0 & 0 & 1 \end{bmatrix}$$

The translation vectors are

$$\boldsymbol{s_1} = \boldsymbol{T}_1 \begin{bmatrix} 0 \\ s_y \\ 0 \end{bmatrix}, \qquad \boldsymbol{s_2} = \boldsymbol{T}_2 \begin{bmatrix} 0 \\ s_y \\ 0 \end{bmatrix}$$

With the rotation matrices, and the cross product matrix of the translation vectors, an adjoint transformation matrix is obtained for both flexure elements, $\boldsymbol{Ad}_1$ and $\boldsymbol{Ad}_2$ respectively. Since both flexure elements are identical, their compliance matrix $\boldsymbol{C}$ is also identical when expressed in their local coordinate system respectively. The compliance matrices of the flexure elements can now be expressed in the global coordinate system as

$$\boldsymbol{C}_1 = \boldsymbol{Ad}_1 \boldsymbol{C} \boldsymbol{Ad}_1^T, \quad \text{and} \quad \boldsymbol{C}_2 = \boldsymbol{Ad}_2 \boldsymbol{C} \boldsymbol{Ad}_2^T$$

Adding the compliances of each flexure elements according to the rules for serial linkages gives $\boldsymbol{C}_t$, and the inverse gives the stiffness matrix $\boldsymbol{K}_t$ of the parallel mechanism.

$$\boldsymbol{C}_t = \left(\boldsymbol{C}_1^{-1} + \boldsymbol{C}_2^{-1}\right)^{-1}$$

$$\boldsymbol{K}_t = \boldsymbol{C}_t^{-1}$$

The matlab code used for transformation and combination of the flexure elements in parallel can be found in Appendix G.2

D Derivation of compliance matrix for case study three

The mechanism discussed in Appendix C can also be analyzed as a serial linkage of two leaf flexures. The face of one of the flexure elements that was considered to be fixed to the ground, now becomes the free end of the serial linkage. What was first the EE, now becomes an intermediate body. The serial linkage is portrayed in Figure 14 with its local coordinate systems, $l_1m_1n_1$, $l_2m_2n_2$, and its global coordinate system x_1, y_1, z_1. The origin of the global coordinate system coincides with the origin of local coordinate system 2. The flexures are both orientated with an angle θ from the intermediate body. The distance between the two flexures at the intermediate body is 20 mm.

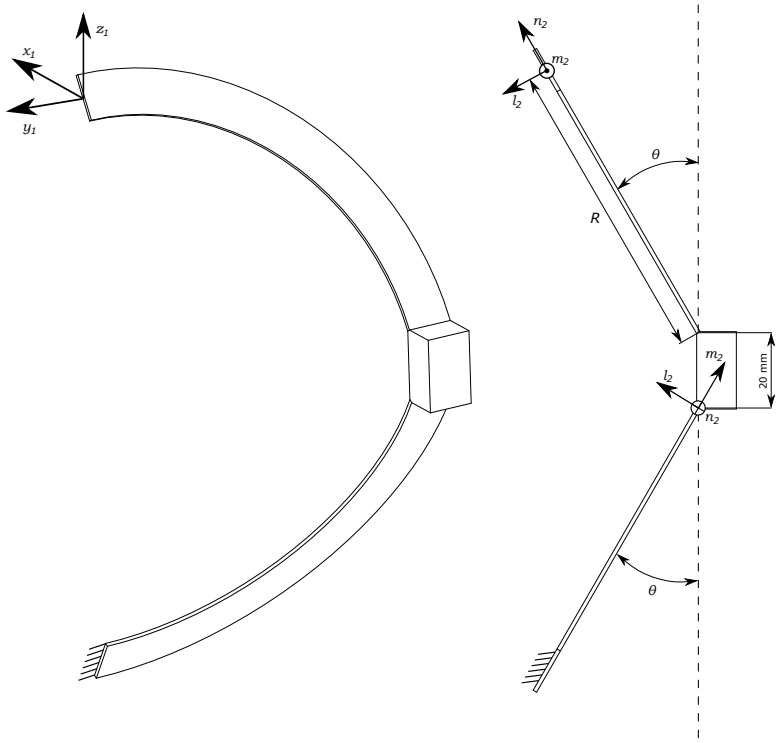

Figure 14: Serial linkage of two CCLF (left), and its side view (right)

The transformation from the local coordinate systems $l_1m_1n_1$ and $l_2m_2n_2$ to the global coordinate system $x_1y_1z_1$ is described by the rotation matrices $\boldsymbol{T}_1$ and $\boldsymbol{T}_2$, and the translation vectors $\boldsymbol{s}_1$ and $\boldsymbol{s}_2$.

$$\boldsymbol{T}_1 = \begin{bmatrix} \cos(\theta) & -\sin(\theta) & 0 \\ 0 & 0 & -1 \\ \sin(\theta) & \cos(\theta) & 0 \end{bmatrix}, \qquad \boldsymbol{T}_2 = \begin{bmatrix} \cos(\theta) & \sin(\theta) & 0 \\ 0 & 1 & 0 \\ -\sin(\theta) & \cos(\theta) & 0 \end{bmatrix}$$

$$\boldsymbol{s_1} = \begin{bmatrix} 0 \\ 0 \\ 0 \end{bmatrix}, \qquad \boldsymbol{s_2} = \begin{bmatrix} R\sin(\theta) \\ R \\ 20\,\mathrm{mm} + R\cos(\theta) \end{bmatrix}$$

Using $\boldsymbol{T}_1$, $\boldsymbol{T}_2$, and the cross product matrices of $\boldsymbol{s}_1$ and $\boldsymbol{s}_2$, adjoint transformation matrices $\boldsymbol{Ad}_1$ and $\boldsymbol{Ad}_2$ can be formed. The compliance matrix of the serial linkage expressed in $x_1y_1z_1$ can be obtained as

$$\boldsymbol{C}_{serial\,leg} = \boldsymbol{Ad}_1\boldsymbol{C}\boldsymbol{Ad}_1^T + \boldsymbol{Ad}_2\boldsymbol{C}\boldsymbol{Ad}_2^T$$

For a serial linkage, the constraints are determined by the constraints that each flexure element shares. In this case it means that the serial linkage has one linear constraint in y_1. By combining the three serial linkages in parallel, a new mechanism emerges. As shown in Figure 15, the serial linkages are combined at an EE, circularly patterned around the Z-axis of the new global coordinate system XYZ under an angle $\alpha = 120°$. The transformation from each serial linkage is described in the transformation matrices $\boldsymbol{T}_{\mathrm{I}}$, $\boldsymbol{T}_{\mathrm{II}}$, and $\boldsymbol{T}_{\mathrm{III}}$, and the translation vectors $\boldsymbol{s}_1$, $\boldsymbol{s}_2$, and $\boldsymbol{s}_3$.

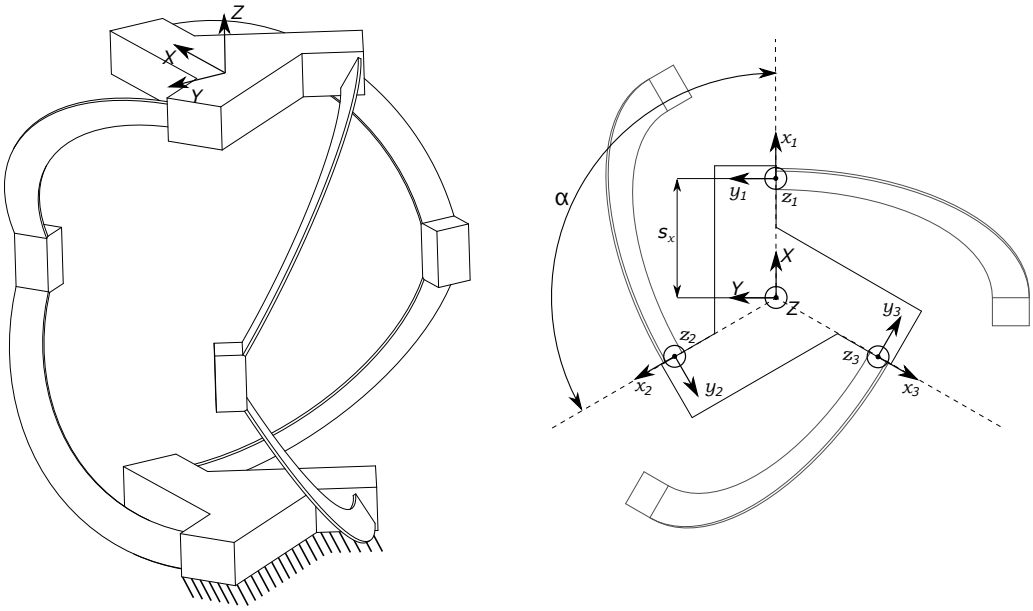

Figure 15: Parallel mechanism consisting of three serial linkages of CCLF (left), and a top view of the mechanism (right).

$$\boldsymbol{T}_{\mathrm{I}} = \begin{bmatrix} 1 & 0 & 0 \\ 0 & 1 & 0 \\ 0 & 0 & 1 \end{bmatrix}, \qquad \boldsymbol{T}_{\mathrm{II}} = \begin{bmatrix} \cos(\alpha) & -sin(\alpha) & 0 \\ \sin(\alpha) & \cos(\alpha) & 0 \\ 0 & 0 & 1 \end{bmatrix}, \qquad \boldsymbol{T}_{\mathrm{III}} = \begin{bmatrix} \cos(\alpha) & sin(\alpha) & 0 \\ -\sin(\alpha) & \cos(\alpha) & 0 \\ 0 & 0 & 1 \end{bmatrix}$$

The translation from the origin of the local coordinate system to the global coordinate system is identical for each flexure element due to symmetry. The distance from the origin of $x_1y_1z_1$, $x_2y_2z_2$, and $x_3y_3z_3$ to the origin of global coordinate system XYZ is $s_x = 20\,\mathrm{mm}$ expressed in their respective local coordinate systems. $\boldsymbol{s}_{\mathrm{I}}$, $\boldsymbol{s}_{\mathrm{II}}$, and $\boldsymbol{s}_{\mathrm{III}}$ give the translation vectors of the free end of each leg to the origin of XYZ in the global coordinate system.

$$\boldsymbol{s_I} = \boldsymbol{T}_{\mathrm{I}} \begin{bmatrix} -s_x \\ 0 \\ 0 \end{bmatrix}, \qquad \boldsymbol{s}_{\mathrm{II}} = \boldsymbol{T}_{\mathrm{II}} \begin{bmatrix} -s_x \\ 0 \\ 0 \end{bmatrix}, \qquad \boldsymbol{s}_{\mathrm{III}} = \boldsymbol{T}_{\mathrm{III}} \begin{bmatrix} -s_x \\ 0 \\ 0 \end{bmatrix}$$

With the above transmormation matrices and translation vectors, the adjoint transformation matrices $\boldsymbol{Ad}_{\mathrm{I}}$, $\boldsymbol{Ad}_{\mathrm{II}}$, and $\boldsymbol{Ad}_{\mathrm{III}}$ can be formed, which transform the compliance matrix of leg $\mathrm{I}, \mathrm{II}, and \mathrm{III}$ to the origin of the global coordinate system XYZ.

$$\begin{aligned} \boldsymbol{C}_{leg\mathrm{I},\, global} &= \boldsymbol{Ad}_{\mathrm{I}} \boldsymbol{C} \boldsymbol{Ad}_{\mathrm{I}}^T \\ \boldsymbol{C}_{leg\mathrm{II},\, global} &= \boldsymbol{Ad}_{\mathrm{II}} \boldsymbol{C} \boldsymbol{Ad}_{\mathrm{II}}^T \\ \boldsymbol{C}_{leg\mathrm{III},\, global} &= \boldsymbol{Ad}_{\mathrm{III}} \boldsymbol{C} \boldsymbol{Ad}_{\mathrm{III}}^T \end{aligned}$$

Now the compliance matrix of the entire mechanism, consisting of the three serial legs in parallel can be achieved as

$$\boldsymbol{C}_{total} = \left((\boldsymbol{C}_{leg\mathrm{I},\, global})^{-1} + (\boldsymbol{C}_{leg\mathrm{II},\, global})^{-1} + (\boldsymbol{C}_{leg\mathrm{III},\, global})^{-1} \right)^{-1}$$

The matlab code used for transformation and combination of the flexure elements in series and parallel for this mechanism can be found in Appendix G.3

E FEM validation

In order to validate the analytical model, it has been compared with a finite element analysis (FEA). The mesh of the FEA model consists of second order mesh elements, as a short computation time is not a priority. Since the analytical model does not consider non-linearities, it should only be used for small deformations. Therefore, a linear FEA is sufficient for the validation of the results. Since the FEA is used to test the results from the analytical model, the FEA should be validated too. This is achieved by a mesh convergence study. The mesh is refined by reducing the element size, through which the number of mesh elements increases. For each mesh refinement, the results are compared with the results from the previous mesh. The error between these results is determined as

$$\text{error} = 100\left(\frac{\Delta_i - \Delta_{i-1}}{\Delta_{i-1}}\right)$$

Here, Δ is the result from the FEA, and i indicates the refinement step. Mesh convergence is assumed when the results of two consecutive refinements do not vary more than 1 %. For the refinement, not only the mesh size is reduced, but also the number of mesh elements in the width of the flexure is increased. Figure 16 shows how the mesh is refined for two refinement steps.

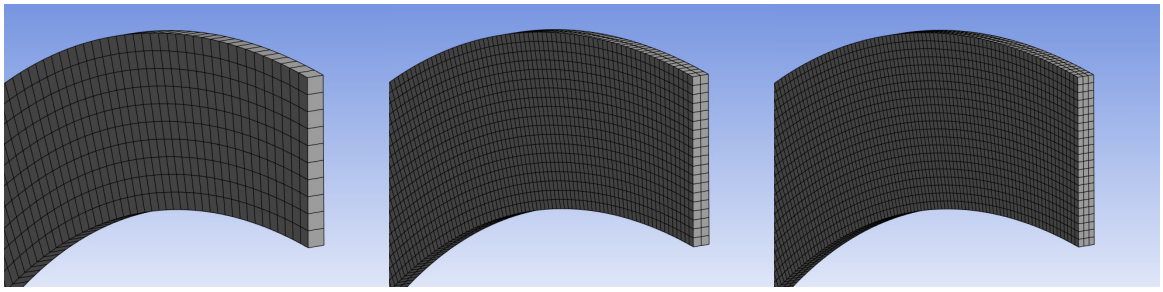

Figure 16: The change in the mesh for two refinement steps.

As shown in Appendix A, the compliance matrix is symmetric, and therefore has 12 independent elements. In order to validate the analytically obtained compliance matrix of a particular geometry, each of these 12 elements should converge. Figure 17 illustrates the convergence of matrix element K_{x,f_x} of the transformation matrix for a flexure with a length L= 150 mm, a sweep angle ϕ= 90 °, and a height h= 15 mm.

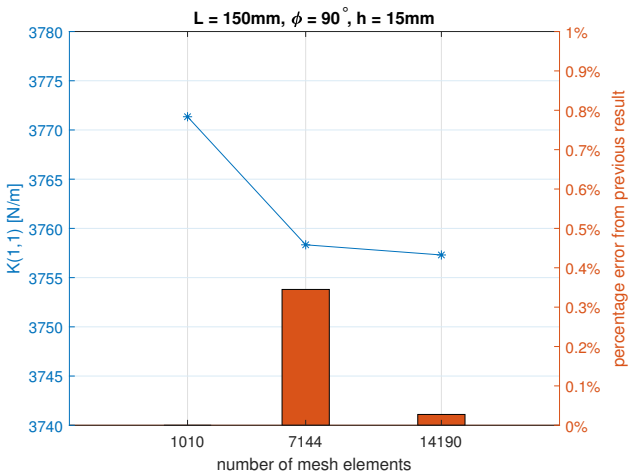

Figure 17: The convergence of FEA results and its percentage difference.

F Test setup

An experimental setup was build to compare the result of physical flexures with the results from the FEA and the analytical model. In order to measure the stiffness in a certain direction, motion in the other directions needs to be constrained. To do this, an end effector (EE) has been designed, which can be attached to a linear or rotary bearing. Since these bearings constrain five directions of motion, a single motion remains free. The stiffness in the direction of motion which is free is therefore isolated and can be measured. The orientation of the bearings with respect to the EE can be changed. Allowing for the measurement in different directions. By displacing the EE with a PI stage, a deflection of the flexure is evoked. The load sensor, which is positioned between the EE and the PI stage measures the load. With both the load from the load sensor and the displacement of the PI stage, a load deflection curve can be plotted, from which the stiffness can be determined.

F.1 Single flexure

For the single flexure, measurements were done for one translational stiffness and two rotational stiffnesses. Figure 18 shows the EE that was used to constrain all motions, except a rotation around z. The Flexure is clamped between EE1 and EE2. To attach the rotary bearings to EE1, EE2 and EE3 were printed using PLA. The bearings are press fitted in EE3, and an M6 bolt is passed through the bearings and fixed to the world. EE2 provides the connection of EE3 with EE1, and is open in its center to allow the head of the M6 bolt. EE3 shows an elongated body to provide a lever, which is necessary to create a rotation, and measure a moment around the rotation axis. At first, EE1 and EE2 were made from PLA using fused deposition modeling 3D printing, which showed to have insufficient stiffness to effectively clamp the flexure. Therefore EE1 and EE2 has been made from aluminium.

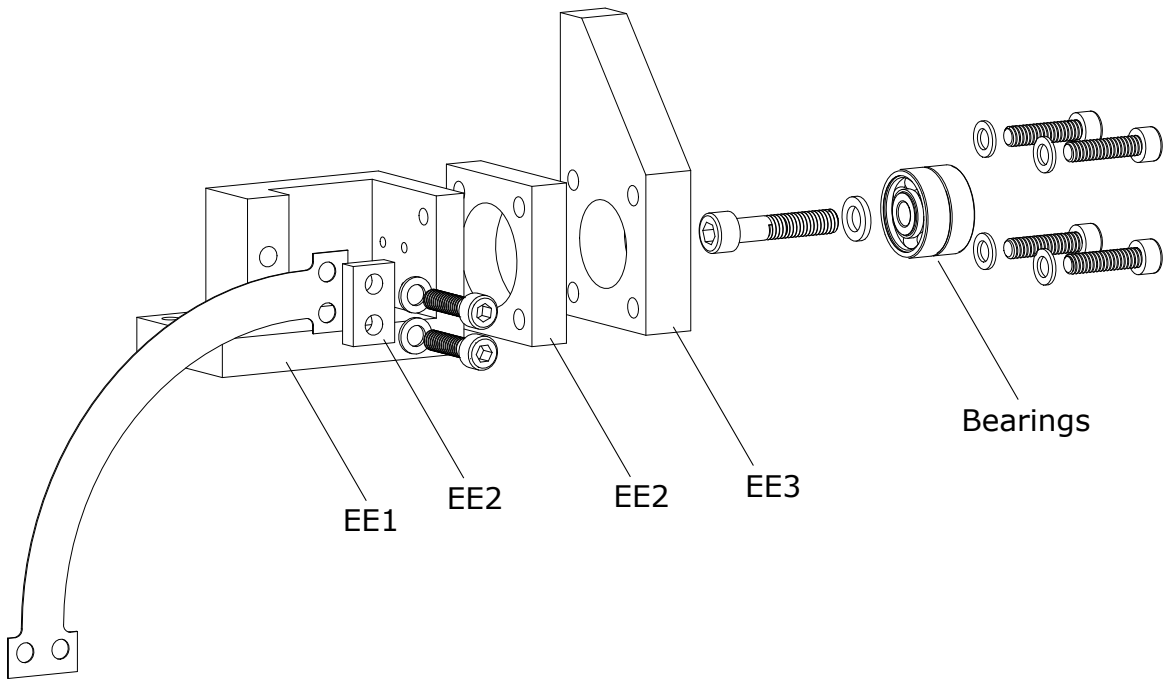

Figure 18: The assembly of the EE and a rotary bearing, for a measurement of the rotational stiffness around z for a single flexure.

By orientating EE2, and EE3 including the bearings differently with respect to EE1, a rotation around a different axis of the flexure is allowed. Also, a linear bearing can be attached to EE1 directly, as is shown in Figure 4. The other end of the flexure was fixed to the ground using mechanical clamps.

F.2 Parallel mechanism

To measure the rotational stiffness of the parallel mechanism containing two CCLF, an EE needed to be fabricated that can effectively clamp the two CCLF under an angle, and allows for the rotary bearing to be

attached. For this, only EE1 needs to be changed with respect to the end effector of the single flexure. With its slightly more complex geometry, the EE was fabricated with a resin printer. The resin, *Formlabs RIGID 10K*, was used, which has a Young's modulus of $E = 10\,\text{GPa}$. Due to limited space, the flexures were attached to the new EE with bolts and threaded holes in the EE. EE2 and EE3 are attached to the new EE as was done with the single flexure. The new EE, connecting two CCLF to a base is shown in Figure 19. A linear or rotary bearing can be attached to the EE with different orientations.

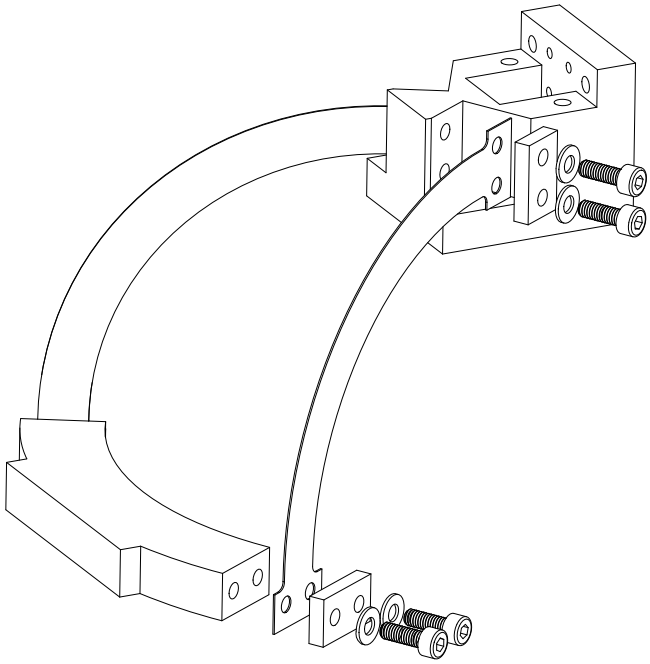

Figure 19: The assembly of the EE and a rotary bearing, for a measurement of the rotational stiffness around z for a parallel mechanism with two CCLF.

G Matlab code

G.1 Matlab code for the derivation of a single CCLF

```
%% This script creates a parametric closed form compliance matrix of a single CCLF using the direct method
syms phi R A              % The sweep angle, radius, and cross section area
syms I_n I_l J real       % The area moments of inertia, and torsion constant
syms E G B_n B_l real     % The Young's modulus, shear modulus, and shear coefficients
% Vector r from the origin of xyz at the free end to the origing of lmn
% along the centroidal curve of the flexure
r = [0;
     -R*sin(phi);
     -R + R*cos(phi)];

% Cross product matrix of vector r
D = [0 -r(3) r(2);
     r(3) 0 -r(1);
     -r(2) r(1) 0];

% Rotation matrix from local to global coordinate system
T = [1 0 0;
     0 cos(phi) -sin(phi);
     0 sin(phi) cos(phi)];

% Transformation matrix from the global to the local coordinate system
B = [T' zeros(3,3);
     T'*-D T'];

% Rigidity matrix of element ds
xi = [B_l*G*A   0       0       0       0       0;
        0      E*A      0       0       0       0;
        0       0    B_n*G*A    0       0       0;
        0       0       0     E*I_l     0       0;
        0       0       0       0     G*J       0;
        0       0       0       0       0    E*I_n];

C = B'*inv(xi)*B*R;
C = simplify(C);

% Integrate over [0, phi] for varial of integration phi
C = simplify(int(C,phi, 0, phi));

% Save the parametric compliance matrix for later use
save("C","C")
```

G.2 Matlab code for the derivation of the parallel mechanism containing two CCLF (case study 2)

Compliance matrix C should be substituted with numerical parameters before transformations, to prevent large parametric matrix elements and long running times.

```
%% In this matlab file, the compliance matrix of a parallel mechanism consisting of two CCLF will be derived
%  The parallel mechanism concerns the one discussed in case study two (Section 3.2)

% First, the compliance matrix of a single CCLF is loaded. This compliance
% matrix is expressed in the local coordinate system at its free end.
load("C");

% Introduce the necessary symbolic variables
syms theta real      % The angle between the two CCLF
syms sy real         % The distance from the origin of the local coordinate system to the global coordinate system

% Rotation matrices T1 and T2 from the local coordinate system of flexure 1
% and flexure 2 to the global coordinate system
T1 = [cos(theta/2) -sin(theta/2) 0;
      sin(theta/2) cos(theta/2) 0;
      0 0 1];

T2 = [cos(theta/2) sin(theta/2) 0;
      -sin(theta/2) cos(theta/2) 0;
      0 0 1];

% Translation vectors s1 and s2 from the origin of the local to the origin
% of the global coordinate system, expressed in the global coordinate
% system
s1 = T1*[0;
         sy;
         0];
s2 = T2*[0;
         sy;
         0];

% Cross product matrices D1 and D2 of s1 and s2 respectively
D1 = [0 -s1(3) s1(2);
      s1(3) 0 -s1(1);
      -s1(2) s1(1) 0];
D2 = [0 -s2(3) s2(2);
      s2(3) 0 -s2(1);
      -s2(2) s2(1) 0];

% Adjoint transformation matrices Ad1 and Ad2 respectively
Ad1 = [T1 D1'*T1;
       zeros(3) T1];
Ad2 = [T2 D2'*T2;
       zeros(3) T2];

% The compliance matrix of flexure 1 and 2, expressed in the global
% coordinate system, after transformation by the adjoint transformation
% matrix
```

```
C1 = Ad1*C*Ad1';
C2 = Ad2*C*Ad2';

% The stiffness matrix of both flexures, expressed in the global coordinate
% system
K1 = inv(C1);
K2 = inv(C2);

% As it concerns a parallel mechanism, K1 and K2 can be summed up to obtain
% the stiffness matrix of the parallel mechanism
Kt = K1+K2

% The inverse of the stiffness matrix gives the compliance matrix of the
% parallel mechanism
Ct = inv(Kt);
```

G.3 Matlab code for the derivation of the three legged mechanism containing three legs of serial CCLF (case study 3)

Compliance matrix C should be substituted with numerical parameters before transformations, to prevent large parametric matrix elements and long running times.

```
%% In this matlab file, the compliance matrix of a parallel mechanism consisting
    of three legs of serial CCLF will be derived
%  The parallel mechanism concerns the one discussed in case study three (
    Section 3.3)

% First, the compliance matrix of a single CCLF is loaded. This compliance
% matrix is expressed in the local coordinate system at its free end.
load("C");

%%%% Compliance matrix of a leg containing two CCLF %%%%
% Introduce the necessary symbolic variables
syms theta real      % The angle between the CCLF and the intermediate body
syms L_ib            % The length of the intermediate body

% Rotation matrices T1 and T2 from the local coordinate system of the two
% CCLF in the serial leg to the global coordinate system 'x1y1z1' at the
% free end of the upper flexure
T1 = [cos(theta/2) -sin(theta/2) 0;
      0 0 -1;
      sin(theta/2) cos(theta/2) 0];

T2 = [cos(theta/2) 0 sin(theta/2);
      0 1 0;
      -sin(theta/2) 0 cos(theta/2)];

% Translation vectors s1 and s2 from the origin of the local to the origin
% of the global coordinate system, expressed in the global coordinate
% system
s1 = [R*sin(theta/2);
      R;
      R*cos(theta/2) + L_ib];

s2 = [0; 0; 0];

% Cross product matrices D1 and D2 of s1 and s2 respectively
D1 = [0 -s1(3) s1(2);
      s1(3) 0 -s1(1);
      -s1(2) s1(1) 0];
D2 = [0 -s2(3) s2(2);
      s2(3) 0 -s2(1);
      -s2(2) s2(1) 0];

% Adjoint transformation matrices Ad1 and Ad2 respectively
Ad1 = [R1 D1'*R1;
       zeros(3) R1];
Ad2 = [R2 D2'*R2;
       zeros(3) R2];

% The compliance matrices of the flexure elements expressed in the
% coordinate system of the serial leg
C1 = Ad1*C*Ad1';
```

```
C2 = Ad2*C*Ad2';

% The comliance matrix of a leg containing two CCLF
Cserial = C1 + C2;

%%%%% Compliance matrix of three legs in parallel %%%%%
% Introduce the necessary symbolic variables
syms alpha real      % The angle between two legs
syms sx              % The distance between the coordinate system of a leg, and the global coordinate system

% Rotation matrices T_I, T_II, and T_III from the coordinate system of a
% single leg, to the global coordinate system XYZ
T_I = [1 0 0; 0 1 0; 0 0 1];
T_II = [-sin(alpha) -cos(alpha) 0; cos(alpha) -sin(alpha) 0; 0 0 1];
T_III = [-sin(alpha) cos(alpha) 0; -cos(alpha) -sin(alpha) 0; 0 0 1];

% Translation vectors s_I, s_II, and s_III from the coordinate system of a
% single leg, to the global coordinate system XYZ, expressed in the global
% coordinate system
s_I = T_I*[-sx; 0; 0];
s_II = T_II*[-sx; 0; 0];
s_III = T_III*[-sx; 0; 0];

% Cross product matrices DI, D_II, and D_III of s_I, s_II, and s_III respectively
D_I = [0  -s_I(3)  s_I(2);
       s_I(3)  0  -s_I(1);
      -s_I(2)  s_I(1)  0];
D_II = [0  -s_II(3)  s_II(2);
        s_II(3)  0  -s_II(1);
       -s_II(2)  s_II(1)  0];
D_III = [0  -s_III(3)  s_III(2);
         s_III(3)  0  -s_III(1);
        -s_III(2)  s_III(1)  0];

% Adjoint transformation matrices Ad_I, Ad_II, and Ad_III respectively
Ad_I = [T_I  D_I'*T_I;
        zeros(3) T_I];
Ad_II = [T_II  D_II'*T_II;
         zeros(3) T_II];
Ad_III = [T_III D_III'*T_III;
          zeros(3) T_III];

% The compliance matrix of the three legs, expressed in the global
% coordinate system, after transformation by their respective adjoint
% transformation matrix
C_I = Ad_I*Cserial*Ad_I';
C_II = Ad_II*Cserial*Ad_II';
C_III = Ad_III*Cserial*Ad_III';

% Obtaining the compliance matrix of the mechanism (Ct) by adding up the
% stiffness matrices
K_I = inv(C_I); K_II = inv(C_II); K_III = inv(C_III);
Kt = K_I + K_II + K_III;
Ct = inv(Kt);
```